Review

# Review of electronic transport models for thermoelectric materials

A. Bulusu[a], D.G. Walker[b],*

[a] Interdisciplinary Program in Materials Science, Vanderbilt University, VU Station B 351592, 2301 Vanderbilt Place, Nashville, TN 37235, United States
[b] Department of Mechanical Engineering, Vanderbilt University, VU Station B 351592, 2301 Vanderbilt Place, Nashville, TN 37235, United States

## Abstract

Thermoelectric devices have gained importance in recent years as viable solutions for applications such as spot cooling of electronic components, remote power generation in space stations and satellites etc. These solid-state devices have long been known for their reliability rather than their efficiency; they contain no moving parts, and their performance relies primarily on material selection, which has not generated many excellent candidates. Research in recent years has been focused on developing both thermoelectric structures and materials that have high efficiency. In general, thermoelectric research is two-pronged with (1) experiments focused on finding new materials and structures with enhanced thermoelectric performance and (2) analytical models that predict thermoelectric behavior to enable better design and optimization of materials and structures. While numerous reviews have discussed the importance of and dependence on materials for thermoelectric performance, an overview of how to predict the performance of various materials and structures based on fundamental quantities is lacking. In this paper we present a review of the theoretical models that were developed since thermoelectricity was first observed in 1821 by Seebeck and how these models have guided experimental material search for improved thermoelectric devices. A new quantum model is also presented, which provides opportunities for the optimization of nanoscale materials to enhance thermoelectric performance.
© 2008 Elsevier Ltd. All rights reserved.

## Contents

* Corresponding author. Tel.: +1 615 343 6959; fax: +1 615 343 6687.
  *E-mail addresses:* anuradha.bulusu@vanderbilt.edu (A. Bulusu), greg.walker@vanderbilt.edu (D.G. Walker).

## 1. Thermoelectric properties

When two ends of a wire are held at different temperatures, a voltage develops across the two sides. This effect is known as the Seebeck effect, which was discovered by Seebeck in 1821 and published in 1822 [1]. The voltage between the two ends is proportional to the temperature difference across the wire provided the temperature gradient is small. The proportionality constant is defined as the Seebeck coefficient or thermoelectric power and is obtained from the ratio of the voltage generated and the applied temperature difference.

$$S = \frac{\Delta V}{\Delta T}. \tag{1}$$

In 1834, the Peltier effect, a companion to the Seebeck effect, was discovered [2]. This effect occurs when a current passes through a wire. The current will carry thermal energy so that the temperature of one end of the wire decreases and the other increases. The Peltier coefficient $\Pi_{12}$ is defined as the heat emitted per unit time per unit current flow from conductor 1 to 2. Therefore, this heat is directly proportional to the current passing through the junction as described by Eq. (2).

$$\mathrm{d}Q = \prod \mathrm{d}I. \tag{2}$$

The Peltier effect is often overwhelmed by irreversible Joule heating, which also originates from electronic current. The Thomson effect was predicted in 1854 and found experimentally in 1856 [3]. The Thomson effect occurs when a current flows across two points of a homogeneous wire having a temperature gradient along its length and heat is emitted or absorbed in addition to the Joule heat. The Thomson coefficient $\mu_T$ is positive if heat is generated when positive current flows from a higher temperature to lower temperature.

$$\mathrm{d}Q = \mu_T \frac{\partial T}{\partial x} \mathrm{d}x \mathrm{d}I. \tag{3}$$

The three thermal–electrical properties provide the basis for modern direct energy conversion devices and their exploitation has been the subject of considerable research. In 1912, Altenkirch [4,5] introduced the concept of a figure of merit when he showed that good thermoelectric materials should possess large Seebeck coefficients, high electrical conductivity to minimize Joule heating and low thermal conductivity to retain heat at the junctions that will

**Nomenclature**

| | |
|---|---|
| $S$ | Seebeck coefficient |
| $\Pi_{12}$ | Peltier coefficient |
| $\mu_T$ | Thomson coefficient |
| $\sigma$ | Electrical conductivity |
| $\kappa$ | Thermal conductivity |
| $ZT$ | Thermoelectric figure of merit |
| $Q$ | Thermal current |
| $J$ | Electric current density |
| $\mu$ | Carrier mobility |
| $e$ | Charge of an electron |
| $m_e$ | Mass of an electron |
| $n_e$ | Electron concentration |
| $l_e$ | Electron mean free path |
| $l_p$ | Phonon mean free path |
| $\tau$ | Phonon relaxation time |
| $c$ | Crystal specific heat |
| $\upsilon_s$ | Velocity of sound |
| $\nu$ | Electron velocity |
| $\rho_m$ | Crystal mass density |
| $k_B$ | Boltzmann constant |
| $h$ | Planck's constant |
| $\lambda$ | de Broglie wavelength |
| $f_0$ | Fermi–Dirac distribution |
| $\varepsilon_r$ | Dielectric constant |
| $Eg$ | Bandgap energy |
| $a_{Eg}$ | Parameter to measure temperature variation of bandgap |
| $Ec$ | Conduction band edge |
| $\varepsilon$ | Electron energy |
| $\varepsilon_f$ | Fermi energy |
| $r$ | Scattering parameter |
| $I$ | Electric current |
| s | Entropy |
| $U_i$ | Internal energy |
| $\beta$ | Material parameter — Chasmar and Stratton |
| $\beta_0$ | Material parameter — Mahan |
| $B$ | Material parameter — Dresselhaus and Hicks |
| $\gamma$ | Material parameter — Simon |
| $k_\parallel$ | In-plane wave vectors |
| $k_\perp$ | Cross-plane wave vectors |
| $H$ | Hamiltonian function |
| $U$ | Hartree potential |
| $\psi$ | Wave function |
| $G(\varepsilon)$ | Retarded Green's function |
| $G^+(\varepsilon)$ | Advanced Green's function |

| $G^n(\varepsilon)$ | Electron density matrix |
| $A(\varepsilon)$ | Electron density of states matrix |
| $\Sigma$ | Self-energy matrix |
| $\Gamma$ | Broadening matrix |
| $Nd$ | Doping density |
| $\omega_0$ | Phonon frequency |
| $D_0$ | Optical-phonon deformation potential |

help maintain a large temperature gradient. Ioffe in 1957 [6] presented the figure of merit as $Z = S^2\sigma/\kappa$ which he used to qualify the efficiency of thermoelectric materials. The present day dimensionless figure of merit is commonly represented as $ZT = S^2\sigma T/\kappa$.

## 2. Development of semiconductor thermoelectric materials

Initial thermoelectric materials studied were metals, which display Seebeck coefficients of a few tens of µV/K. However, in the middle of the 20th century, interest turned towards semiconductors as thermoelectric materials despite small ratios of electrical to thermal conductivity, due to their high Seebeck coefficients and heat conduction dominated by phonon transport. In 1952 Ioffe [7] studied the change in semiconductor thermal conductivity of a material relative to its position in the periodic table. He found that for larger mean atomic weight, the thermal conductivity was lower. This behavior was attributed to the increase in density that caused the velocity of sound in the crystal to decrease leading to a subsequent decrease in thermal conductivity. Since mobility of electrons serves as a direct relation between the crystal structure and electrical conductivity, Goldsmid [8] studied the ratio of mobility $\mu$ and thermal conductivity $\kappa$ as a function of the mean atomic weight. Using the relationship proposed by Shockley and Bardeen [9] for mobility in semiconductors and Pierls relationship for thermal conductivity, he calculated the ratio as a function of the electron mean free path $l_e$ and phonon mean free path $l_p$ in crystals.

$$\frac{\mu}{\kappa} = \frac{4e\rho_m}{c\upsilon_s(2\pi m_e k_B T)^{1/2}}\frac{l_e}{l_p}. \tag{4}$$

Here $\rho_m$ is the mass density; $\upsilon_s$ the velocity of sound and $c$ is the specific heat of the crystal; $m_e$ and $e$ are the electron mass and charge respectively. Using material properties measured for some common semiconductors they plotted the above ratio against the mean atomic weight of the semiconductors seen in Fig. 1. Applying the above mentioned selection rules of choosing materials with high Seebeck coefficients and high atomic weights led to the discovery of bismuth telluride ($Bi_2Te_3$) in 1954 by Goldsmid [10] that provided cooling of 26 °C. Bismuth telluride has a hexagonal structure with mixed ionic–covalent bonding along the lattice planes and the weak van der Waals bonding perpendicular to the planes. The hexagonal structure ensures high anisotropy in the lattice conductivity with a factor of 2 decrease in the thermal conductivity in the direction perpendicular to the planes. Bismuth telluride also has a multivalley bandstructure with multiple anisotropic constant energy surfaces that have a small effective mass in one direction and large effective masses in the other two directions. Since smaller effective mass leads to high electron mobility, choosing the appropriate growth direction of bismuth telluride is necessary for good thermoelectric performance.
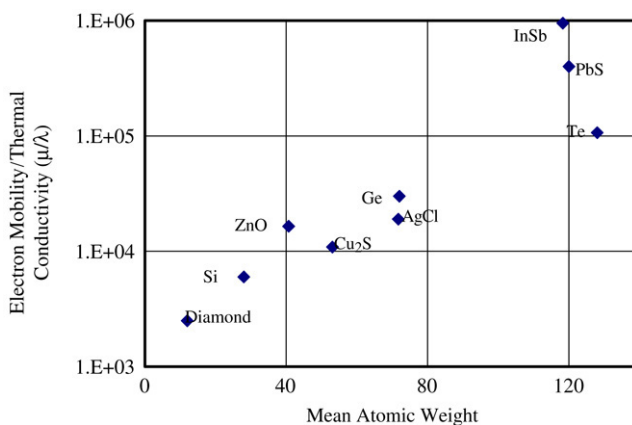
Fig. 1. Ratio of electron mobility to thermal conductivity of thermoelectric materials (reproduced from Ref. [8]).

In 1956, Ioffe et al. [11] suggested that alloying a semiconducting thermoelectric material with an isomorphous substance – materials having the same crystalline structure – would enhance the figure of merit by reducing lattice thermal conductivity without affecting carrier mobility. They suggested that phonons would scatter due to the disturbances in the short-range order but the preservation of long-range order would prevent scattering of electrons and holes. This led to an extensive study of the thermoelectric performance of various semiconductor alloy systems over a wide range of temperatures.

Birkholz in 1958 [12] and Rosi in 1959 [13] showed that alloying $Bi_2Te_3$ with $Sb_2Te_3$ or $Bi_2Se_3$ greatly reduced the thermal conductivity. They also showed that adding even 5% of $Sb_2Se_3$ greatly improved the figure of merit by raising the bandgap that reduced ambipolar conduction i.e. contribution due to both electrons and holes to electrical conductivity and thermal conductivity. These studies led to the formation of a pseudo-ternary $Bi_2Te_3$–$Sb_2Te_3$–$Sb_2Se_3$ system. The studies showed that the best n-type material was the $Bi_2Te_3$ rich alloys while the best p-type performance was obtained from the $Sb_2Te_3$ pseudo-ternary alloys with an average figure of merit of $3.3 \times 10^{-3}$ K$^{-1}$ from both types at room temperature [14]. In general however, bismuth and bismuth telluride alloys are good thermoelectric materials only below room temperature. At room temperature and above, the relatively small bandgap causes mixed conduction due to both electrons and holes leading to reduced Seebeck coefficient.

At temperatures above those that bismuth telluride can be used, materials like lead telluride are found to have very good thermoelectric properties in the range of 300–700 K. Lead telluride belongs to the lead chalcogenides system similar to materials such as PbS and PbSe. Lead chalcogenides have a cubic (NaCl) rock-salt structure with a FCC unit cell. They are polar semiconductors with a mixed ionic–covalent bond with the electrons traveling mainly in the cation (Pb) sublattice and the holes in the anion chalcogenide sublattice. Similar to bismuth telluride, lead telluride (PbTe) has high mean atomic weight and a multivalley bandstructure. Having slightly higher bandgap of 0.32 eV at 300 K, lead telluride produces higher Seebeck coefficients compared to bismuth telluride. While it has higher lattice thermal conductivity than bismuth telluride at room temperature, it eventually produces higher *ZT* values as the temperature is raised. Lead telluride also forms isomorphous solid solutions with lead selenide and tin telluride leading to lower thermal conductivities and improved *ZT* values. Rosi et al. [14] in 1961 studied the bandgap of the PbTe–SnTe system and determined that band reversal effect actually

causes the bandgap to go to zero at the composition $Pb_{0.4}Sn_{0.6}Te$ and hence recommended that lower compositions of tin telluride would ensure sufficient bandgaps leading to *ZT* values near 1 for n-type PbTe–SnTe alloys at 700 K [15]. Another type of alloy system that gives *ZT* values around 1 for temperature range around 700 K are alloys between $AgSbTe_2$ and GeTe called TAGS [16]. These alloys possess the same rock-salt structure of PbTe over part of the compositional range. When the composition of GeTe is greater than 70%, it transits to a rhombohedral structure. The lattice strain associated with this phase transition is also believed to contribute to reduced lattice thermal conductivity values around 1.5 W/m K. At higher temperature ranges of 600–1300 K, silicon and germanium which are bad thermoelectrics due to their high thermal conductivity at room temperature can be alloyed to obtain SiGe alloy, a far superior material for thermoelectric generation [17]. The large bandgap of silicon makes silicon rich alloys such as $Si_{0.7}Ge_{0.3}$ suitable for high temperature applications since problems with minority carrier dominance do not arise. The large phonon scattering ensures low thermal conductivity without affecting the electron mobility making it possible to obtain *ZT* values of 0.5 and higher [18].

Materials exhibit the highest possible thermal conductivity in the crystalline state and the lowest conductivity in the amorphous state. Based on this concept Slack in 1979 [19] proposed that the smallest possible lattice conductivity can be predicted by setting the mean free path of the phonons equal to that in the amorphous state. This observation prompted extensive research into materials that are termed as phonon glass and electron crystal (PGEC). These materials have very complex structures such as compounds of Borides ($YB_{68}$) [20], compounds of silver–thallium ($TlAsSe_3$) [21] and $H_2O$. These materials contain groups of atoms or molecules that do not have precisely defined positions or orientations. The lack of long-range order causes the atoms or molecules to *rattle* and act as phonon scattering sites reducing the thermal conductivity to around 0.5 W/m K

Another class of materials is called Skutterudites, which are complex materials with a chemical formula of $ReTm_4M_{12}$ where Re is a rare earth element such as lanthanum or cerium, Tm is a transition metal such as cobalt, iron, etc. and M is a metalloid such as phosphor, arsenic, or antimony. Binary skutterudites have the chemical formula of $TmM_3$, and its crystal structure has the unique feature of containing two large empty spaces within each unit cell. While the binary structures have reasonably large Seebeck coefficients around 200 µV/K, they still exhibit very high thermal conductivities [15]. When a rare earth element is mixed with the binary skutterudite, the heavy atom of the rare earth element occupies the empty space of the crystal [22]. In addition to causing large impurity scattering of phonons in these materials, the loosely bound heavy atoms rattle in their cages enhancing scattering of phonons and reducing thermal conductivity by an order of magnitude at room temperature. Skutterudites have been found to have a figure of merit greater than unity at temperatures around 700 K.

Additional examples of PGEC materials are inorganic clathrates with the chemical formula $A_8B_{46}$ where B represents for example either gallium or germanium or a combination of the two elements [15]. Clathrates consist of an open framework of gallium and germanium atoms that act as an electron crystal. Guest atoms are selectively incorporated in nanocavities in the crystal. The guest atoms vibrate independent of the crystal structure scattering phonons in the process. These materials are found to be very promising for thermoelectric applications at temperatures above 600 °C. Clathrates can be made of tin, silicon, antimony, etc. Examples of some good thermoelectric clathrates are $Sr_8Ga_{16}Ge_{30}$, $Cs_8Sn_{44}$ as well as $Zn_4Sb_3$ that has been observed to give *ZT* values of 1.3 at 400 K. More recently an alloy of Pb–Sb–Ag–Te abbreviated as LAST was developed as n-type thermoelectric material having *ZT* values around 1.7 [23,24]. These

alloys have nano-sized inclusions during synthesis that act as phonon scattering sites. A similar p-type alloy dubbed as SALT was observed to have $ZT$ values around 1.6, the highest known for p-type thermoelectric materials.

Beyond the development of bulk materials with enhanced thermoelectric properties, superlattices have been proposed as structures that may improve $ZT$. These alternating layers of materials can be manufactured from alloys that are good thermoelectric materials to start with such as $Bi_2Te_3/Sb_2Te_3$, $Bi_2Te_3/Bi_2Se_3$ as well as PbSeTe/PbTe quantum dot superlattices, $Si/Si_{1-x}Ge_x$ and Si/Ge superlattices [25]. By adding interfacial scattering sites, the thermal conductivity of these structures can presumably be reduced. While fabrication of superlattice films and wires can take advantage of the advances made in semiconductor manufacturing technology such as lithography, electroplating, etc., significant challenges exist in translating the high $ZT$ performance of bulk materials into similarly performing nanostructures. In this regard the biggest bottleneck is the electrical conductivity which is dominated by contact resistance. The anisotropic nature of most nanoscale materials also makes their thermal conductivity performance unpredictable and difficult to measure. Measurement of thermoelectric properties at the nanoscale is especially difficult as the substrate and buffer layers can overwhelm the Seebeck coefficient and electrical conductivity measurements. The challenges and high costs associated with nanoscale measurements places special emphasis on the need to have a detailed understanding of electron–hole–phonon transport at the nanoscale for a better prediction of thermoelectric performance. The models used to predict thermoelectric parameters must include the effect of various factors such as electron and phonon mean free paths, electron mobility, effect of bandgap, substrate strain etc. Moreover, quantum confinement effects in low-dimensional structures, while increasing the density of states per unit volume at the Fermi level, can also lead to reduced electrical conductivity due to the limited energy states available for electron transport. Similarly while phonon scattering and confinement at the superlattice interfaces can lead to reduced thermal conductivity, its impact on electron and hole transport through confined carrier-phonon scattering also has to be better understood. There has never been a greater need for a strong model that can couple both quantum and scattering effects to predict transport behavior in nanoscale devices. In the next few sections, we present a review of the various models used to predict thermoelectric performance of bulk as well as low-dimensional structures with a view to identify and distinguish their ability to incorporate the necessary fundamental physics that guide thermoelectric behavior in materials.

## 3. Development of modeling of thermoelectric coefficients

In 1928, Sommerfeld [26] put forth a comprehensive model on free-electron theory in metals using Fermi–Dirac statistics instead of Maxwellian statistics for the free-electron theory in metals developed by Lorentz. Sommerfeld assumed that only the valence electrons in a metal formed a free-electron gas that obeyed the Fermi–Dirac distribution $f_0$. Sommerfeld [27] studied thermoelectric phenomena in metals where various combinations of the electric current and temperature gradient $\partial T/\partial x$ were applied on a wire. From his calculations he obtained equations for the electrical conductivity $\sigma$, thermal conductivity $\kappa$ and Thomson coefficient $\mu_T$. In all his calculations Sommerfeld assumed conditions of local thermodynamic equilibrium and the number of electrons to be independent of temperature, and the mean free path of the electrons $l_e$ to be independent of their velocity $v$.

$$\sigma = \frac{4\pi e^2}{3m_e}\left(\frac{m_e}{h}\right)^3 \int_0^\infty f_0 \frac{\partial}{\partial v}\left(\ell_e v^2\right) \mathrm{d}v \tag{5}$$

$$\kappa = \frac{4\pi m_e}{6}\left(\frac{m_e}{h}\right)^3\left[\int_0^\infty \ell_e v^5 \frac{\partial f_0}{\partial x}\,\mathrm{d}v - \frac{\int_0^\infty f_0 \frac{\partial}{\partial v}\left(\ell_e v^4\right)\mathrm{d}v}{\int_0^\infty f_0 \frac{\partial}{\partial v}\left(\ell_e v^2\right)\mathrm{d}v}\int_0^\infty \ell_e v^3 \frac{\partial f_0}{\partial x}\,\mathrm{d}v\right] \tag{6}$$

$$\mu_T = \frac{2\pi^2 m_e k_B^2 T \lambda^2}{3eh^2} \tag{7}$$

where $m_e$ is the electron mass, $h$ is the Planck's constant and $\lambda$ is the de Broglie wavelength of electrons.

Bloch [28] solved the wave equation for periodic metallic lattice and showed that if the lattice is perfect, the electron would travel infinitely through it and only by taking into consideration the thermal motion of the lattice and the effect of impurities would finite conductivity be obtained. In addition, Bloch showed that the application of Pauli's exclusion principle eliminated the direct proportionality between the number of free electrons and the electrical conductivity. Conduction under an applied field would then take place only if the final energy levels are unoccupied such that the electrons near the Fermi level can make transitions and take part in conduction. Bloch called these electrons conduction electrons. Based on these ideas Bloch introduced temperature dependence of electronic conduction in metals where the electric resistance varied directly with the absolute temperature for high temperatures and varies as $T^5$ for low temperatures. Bloch's theory of electrical conduction could not be easily extended to semiconductors as it seemed to suggest that a lattice should have nearly infinite conductance at low temperatures while in reality the conductivity of semiconductors is very low at low temperatures due to limited number of free electrons. It also could not explain the non-conductivity of insulators. In 1931, Wilson [29] extended Bloch's theory to semiconductors and developed a formal theory of electron transport in semiconductors and insulators with emphasis on the temperature dependence of electrical conductivity. Wilson's work was further extended to study Hall coefficients and thermoelectric power of semiconductors by Bronstein [30] in 1932 and Fowler [31] in 1933 but neither of the results by these authors were in a form suitable for comparison with direct experimental data or predictions of thermoelectric power from measured Hall and resistivity data.

In his book *The Theory of Metals* in 1953 Wilson [32] gave a comprehensive analysis of the conduction mechanism and thermoelectric performance of metals and semiconductors under the relaxation time approximation taking into account the effect of electron scattering with acoustic and optical phonons and electron–impurity scattering. Based on his calculations, the relaxation time in metals for electron–phonon scattering was calculated to be proportional to $\varepsilon^{3/2}T^{-1}$ where $\varepsilon$ is the electron energy. This relation is the same result that was obtained by Bloch for metals. In the case of semiconductors the distribution of electrons is taken to be $f_0 = \exp^{-(\varepsilon - \varepsilon_f/k_BT)}$ and restricting the phonon energy range to values around the Fermi energy $\varepsilon_f$, Wilson calculated the electrical conductivity $\sigma$ to be proportional to $n_e m_e^{*-5/2}T^{-3/2}$ where $m_e^*$ is the effective mass of the electron and $n_e$ is the number of free electrons. By arriving at a direct proportionality between the electrical conductivity and number of free electrons, Wilson was able to show that semiconductors have very low conductivity at low temperatures due to the very small number of free electrons available for conduction.

In 1953 Johnson and Lark-Horovitz [33] used Sommerfeld's model of electric current and thermal current to calculate thermoelectric coefficients for three different cases: (1) impurity temperature range where all the carriers are either n-type or p-type such that the concentration of carriers remains constant with temperature until intrinsic carrier effects become important; (2) transition temperature range where in addition to n- and p-type carriers, intrinsic carriers also exist and hence $n_e \neq n_h$; (3) intrinsic temperature range where intrinsic carrier dominates the

electrons and holes from donors and acceptors such that $n_e = n_h$. The authors used Maxwell statistics to describe the carrier distribution in the semiconductors. The mean free path was said to be affected by lattice vibrations where, similar to Sommerfeld, it was expressed to be independent of carrier energy. In the impurity and transition range an additional mean free path due to impurities was included where the mean free path was expressed as a function of carrier kinetic energy $\varepsilon$ as $l_{\text{imp}} = a_{Eg}\varepsilon^2$ where $a_{Eg}$ is the temperature variation of the bandgap width and was found from the measured thermoelectric power curve of intrinsic germanium [33]. The thermoelectric power for polycrystalline germanium having carrier concentrations ranging from $10^{15}$–$7 \times 10^{18}$ cm$^3$ was calculated using these equations and compared to experiments conducted by Lark-Horovitz, Middleton, Miller Scanlon and Walerstein [34] over a temperature range of 78–925 K. For impurity temperature range of approximately 78–300 K there was lot of scatter in the experimental data and the theoretical predictions were not in good agreement with the experiments. In the transition and intrinsic range of temperatures greater than 300 K there was good agreement between experiments and theory. Despite being founded on equilibrium principles, these models were important in establishing limits to the performance of bulk materials as will be shown later.

When Lord Kelvin (Thomson) [35] formulated his theory of thermoelectric phenomena in 1854 he suggested that similar to the reciprocal relations between force and displacement in a mechanical system in equilibrium, there exist reciprocal relations between two or more irreversible transport processes that interfere with each other when they take place simultaneously in a thermodynamic system. Accordingly if $J$ is the electric current due to an applied field and $Q$ the thermal current due to the application of a temperature gradient, then for independent processes the electro-motive force that drives the electric current is given by

$$X_1 = R_1 J \tag{8}$$

where $R_1$ is the resistance to current flow and the force that drives the thermal current is given by

$$X_2 = R_2 Q \tag{9}$$

where $R_2$ is the resistance to the flow of thermal current. However since these two processes mutually interfere with each other, two forces $X_1$ and $X_2$ must be expressed as a combination of the two resistances $R_1$ and $R_2$ as

$$X_1 = R_{11} J + R_{12} Q \tag{10}$$
$$X_2 = R_{21} J + R_{22} Q. \tag{11}$$

Thomson suggested that as long as there is no heat conduction from one part of the circuit to another, $R_{12} = R_{21}$. Thomson's reciprocal relations were examined by Onsager in 1931 [36] who calculated the thermoelectric properties as the entropy flow per particle due to (1) heat flow from high temperature to low temperature and (2) degradation of electrochemical potential energy into heat. From the macroscopic laws governing the thermoelectric process, the electric current J and the thermal current $Q$ were expressed as

$$-J = L_{11} \frac{1}{T} \nabla \mu + L_{12} \nabla \frac{1}{T} \tag{12}$$

$$Q = L_{21} \frac{1}{T} \nabla \mu + L_{22} \nabla \frac{1}{T}. \tag{13}$$

$L_{11}$, $L_{12}$ and $L_{22}$ are called kinetic coefficients and are properties of the medium such as electrical conductivity, thermal conductivity etc and in the absence of a magnetic field, Onsager stated that

$$L_{12} = L_{21}. \tag{14}$$

Callen in 1948 [37] showed that while Onsager's relations strictly referred to specific transient irreversible processes, they could be extended to steady state processes by considering the system to be the limiting case of many small sections, each in local equilibrium. This assumption is incorporated by treating the temperature $T$ and Fermi energy $\varepsilon_f$ as functions of position. Callen pointed out that this assumption was similar to the assumptions made while using the Boltzmann transport equation where the system is assumed to be in local equilibrium by incorporating the deviation from the equilibrium term in the calculations. Here non-equilibrium effects were introduced to the problem.

In 1953 Frederikse [38] noticed large anomalies in the predicted vs. measured thermoelectric power in germanium below temperatures of 200 K. They attributed these anomalies to the assumption of lattice thermal equilibrium commonly made when calculating thermoelectric coefficients. The deviation from the equilibrium of the lattice at low temperatures results in a phonon current that interacts with the electron current. Frederikse modified Lark-Horovitz's model to include an additional term inversely proportional to temperature that would account for the deviation from equilibrium of the lattice at lower temperatures. Onsager's reciprocal relations were used by Price [39] in 1956 where he used a modification of the Johnson–Lark-Horovitz model [40] to calculate the thermoelectric coefficients in isotropic semiconductors. The thermoelectric parameters were calculated phenomenologically as a function of the electron and hole conductivities using average values of the electric and thermal currents.

$$\sigma = \langle J \bullet J \rangle \tag{15}$$

$$S = \frac{1}{\sigma T} \langle J \bullet Q \rangle \tag{16}$$

$$\kappa_e = \frac{1}{T} \langle Q \bullet Q \rangle. \tag{17}$$

The carrier energy was said to be affected by contributions from (1) electrostatic field (2) band edge energies (3) bandgap and at low temperatures (4) entrainment of the lattice energy due to carrier–lattice collisions known as phonon-drag effect where phonons carrying a thermal current tend to drag the electrons with them from the hot side to the cold side [41]. The resulting expression for thermoelectric power was expressed in terms of the electron and hole electrical conductivities as

$$S = \frac{k_B}{2e\sigma} \left[ \alpha \left( \sigma_e - \sigma_h \right) - \sigma \ln \left( \frac{\sigma_e}{\sigma_h} \right) - \sigma \xi \right]$$

$$\text{where } \sigma = \sigma_e + \sigma_h \quad \text{and} \quad \xi = \log \left( \frac{\mu_e}{\mu_h} \left( \frac{m_e}{m_h} \right)^{3/2} \right). \tag{18}$$

Price assumed that the electron and hole mobilities were independent of doping and used the $S$ vs. $\sigma$ plot to graphically obtain the value of $\alpha$, which represents the optimal performance, as shown in Eq. (19). Price showed that the graph (shown in Fig. 2) formed a loop where n-type materials are at the bottom of the loop and p-type materials at the top. The value where $\sigma_e = \sigma_h$
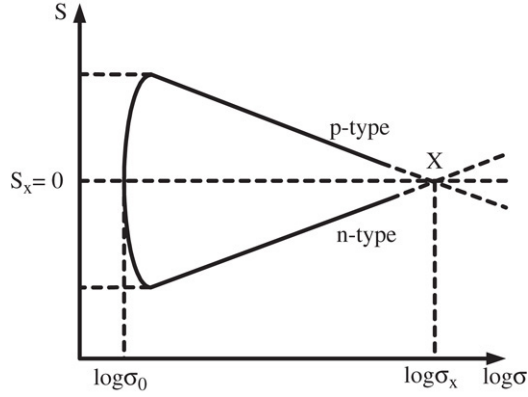
Fig. 2. Price's doping curve for thermoelectric power (reproduced from Ref. [39]).

corresponded to the minimum value of $\sigma$ where minimum thermoelectric power is obtained due to bipolar transport. In addition to the thermoelectric loop, another notable contribution made by Price was the study of the change in thermoelectric power of semiconductors under shear strain. He showed that shear strain would change the activation energy of the impurity donor atom binding a carrier in a many-valley band by decoupling the orbitals associated with the different valleys leading to a shift in the band edge energies. Price recognized that this shift in the band edge energies of the donor atoms would appreciably change the thermoelectric power of semiconductors especially at very low temperatures.

$$\alpha = 2 \log \left( \frac{2\sigma_X}{\sigma_0} \right) \ldots \alpha \gg 1. \tag{19}$$

Ioffe in 1957 [6] gave a simple explanation to calculate the Seebeck coefficient based on thermodynamic considerations. Consider a junction of two conductors through which one coulomb of charge passes at an infinitesimally slow rate such that the current is very small. The entire circuit is assumed to be at constant temperature $T$ such that there is no heat conduction or joule heat loss allowing the system to be treated to be in equilibrium. Since the two conductors are in equilibrium their chemical potentials are equal such that $\varepsilon_{f_1} = \varepsilon_{f_2} = \varepsilon_f$. For a reversible, open system, the definition of internal energy can be written as

$$U_i = Ts + \varepsilon_f. \tag{20}$$

The average energy $U$ as well as the entropy $s$ of the electrons in the two conductors is different. Since the chemical potential of the two conductors is equal, we can write

$$U_{i_1} - Ts_1 = U_{i_2} - Ts_2. \tag{21}$$

When an electron passes through a junction of two conductors its average energy changes by $U_{i1} - U_{i2}$. This difference in electron energy is generated in the form of Peltier heat $\Pi_{1-2}$ at the junction.

$$U_{i_1} - U_{i_2} = \Pi_{1-2}. \tag{22}$$

The relation between Peltier heat and Seebeck coefficient is given by $ST = \Pi_{1-2}$. From Eqs. (21) and (22) the Seebeck coefficient is obtained as

$$S = \frac{\Pi_{1-2}}{T} = \frac{U_{i_1} - U_{i_2}}{T} = S_1 - S_2. \tag{23}$$

Eq. (23) describes the Seebeck coefficient as the flow of entropy per unit charge across a junction. From this definition and Eq. (20), the Seebeck coefficient across the junction can be written as

$$S = \frac{1}{e}\left(\frac{\overline{\varepsilon} - \varepsilon_f}{T}\right) \tag{24}$$

where $\overline{\varepsilon}$ is the average electron energy passing across the junction. If $\varepsilon$ is the energy of each electron passing through the junction and $f(\varepsilon)$ is the distribution function of the electrons, the average electron energy across the junction is calculated as

$$\overline{\varepsilon} = \frac{\int_0^\infty \varepsilon f(\varepsilon)\mathrm{d}\varepsilon}{\int_0^\infty f(\varepsilon)\mathrm{d}\varepsilon}. \tag{25}$$

Using Fermi–Dirac statistics to describe electron distribution in near degenerate semiconductors and a constant relaxation time, power-law approximation to describe carrier energy dependent mean free path of the electrons,

$$\overline{\ell_e} \propto \varepsilon^r. \tag{26}$$

Ioffe calculated the Seebeck coefficient in a semiconductor as

$$S = \frac{k_B}{e}\left[\left(\frac{r+2}{r+1}\right)\frac{f_{r+1}\left(\varepsilon_f/k_B T\right)}{f_r\left(\varepsilon_f/k_B T\right)} - \frac{\varepsilon_f}{k_B T}\right]. \tag{27}$$

The Fermi integrals in Eq. (27) are calculated from

$$f_r\left(\varepsilon_f/k_B T\right) = \int_0^\infty \frac{x^r}{\mathrm{e}^{(x-\varepsilon_f/k_B T)} + 1} \tag{28}$$

where $x = \varepsilon/k_B T$ is the reduced energy for electrons. Ioffe calculated the electrical conductivity through the relation $\sigma = n_e e\mu$, where $n_e$ is the electron density given by Fermi–Dirac statistics as

$$n_e = \frac{4\pi\left(2m_e^* k_B T\right)^{3/2}}{h^3} f_{1/2}\left(\frac{\varepsilon_f}{k_B T}\right) \tag{29}$$

and $\mu$ is the temperature dependent mobility of the electrons. Temperature dependency of mobility was included through the relation $\mu = \mu_0 k_B T^{r+1}$ where $\mu_0$ is the mobility at absolute 0 K. Thermal conductivity was calculated as a sum of the contributions from the electrons as well as lattice vibrations i.e. phonons. The lattice conductivity was obtained from

$$\kappa_{ph} = \frac{1}{3}c\upsilon_s l_p \tag{30}$$

$c$ is the specific heat obtained from the Debye model, $\upsilon_s$ is the sound velocity and $l_p$ is the phonon mean free path. The electron contribution to thermal conductivity calculated from the

general case of the Wiedemann–Franz law is given by

$$\frac{\kappa_{el}}{\sigma} = A \left(\frac{k_B}{e}\right)^2 T \tag{31}$$

The coefficient $A$ accounts for the various scattering mechanisms and is equal to

$$A = \left[\frac{r+3}{r+1}\frac{f_{r+2}\left(\varepsilon_f/k_BT\right)}{f_r\left(\varepsilon_f/k_BT\right)} - \frac{(r+2)^2}{(r+1)^2}\frac{f_{r+1}^2\left(\varepsilon_f/k_BT\right)}{f_r^2\left(\varepsilon_f/k_BT\right)}\right] \tag{32}$$

where the scattering parameter $r$ changes depending on the type of scattering. For example, the value of $r$ is $-1$ for scattering with optical phonons while for ionized-impurity scattering, which is predominant in metals, the value of $r$ is determined to be equal to be 2. This model combines transport concepts with fundamental properties to achieve a reliable estimator of the thermoelectric properties of bulk materials.

In 1959 Chasmar and Stratton [42] used Ioffe's model to calculate the optimum value of the Fermi level that would give the maximum value of $ZT$ for various values of the scattering parameter $r$. Using classical statistics and Fermi–Dirac statistics respectively they obtained the maximum value of $ZT$ as a function of material parameters. They introduced a material parameter $\beta$ which was a function of the effective mass and temperature of the system and the low carrier concentration mobility $\mu$.

$$\beta = \frac{\frac{2e(2\pi m^* k_B T)^{3/2}}{h^3}\left(\frac{k_B}{e}\right)^2 T\mu}{\kappa_l}. \tag{33}$$

For a given temperature and material parameter $\beta$, the optimum value of Fermi energy to maximize $ZT$ was calculated for various scattering parameters $r$. Their calculations indicated that the value of $\beta$ and hence the figure of merit $ZT$ must increase as the temperature rises. More importantly their work was the first to identify the impact of bandgap on the figure of merit. While materials with large bandgaps were found to have low carrier mobility and high thermal conductivity, small bandgap materials would result in low $ZT$ values at high temperatures due to increased minority carrier contribution to thermal conductivity. In addition ionic compounds were shown to be poor thermoelectric materials due to very high polar scattering of electrons, which decreases mobility. Chasmar and Stratton combined their analysis with the results of Goldsmid [8] whose studies on the ratio of mobility to thermal conductivity as a function of the atomic weight led to the discovery of bismuth telluride. From their analysis semiconductors with optimal values of $\beta$ between 0.1 and 0.2 and high atomic weight include sulphides, selenides and tellurides of heavy metals such as lead or bismuth. Though these compounds have low bandgap at 0 K ($\leqslant$0.22 eV), the bandgap increases with temperature. Cadmium telluride on the other hand has a large bandgap, 1.45 eV at 300 K but the material parameter $\beta$ is only 0.03–0.06. Based on the above studies Chasmar and Stratton proposed that a combination of cadmium telluride or selenide (large bandgap, small $\beta$) with a telluride or selenide of small bandgap and large $\beta$ would result in a good thermoelectric material.

Attempts to find an upper bound to the figure of merit were made by various researchers. Littman and Davidson [43] used irreversible thermodynamics to show that no upper limit was imposed on $ZT$ by the second law. However, Rittner and Neumark [44] showed that it was important to employ a combination of statistical or kinetic methods with a proper physical model of semiconductors to study the figure of merit. Simon [45] studied the optimum $ZT$ value in

two band semiconductors as a function the minimum bandgap $E_g$, material parameter $\beta$ for electrons and holes and the scattering parameter $r$ for electrons and holes. He defined a parameter $\gamma = (m_e/m_h)^{3/4}(\mu_e/\mu_h)^{1/2}$ that he varied by adjusting the material parameters $\beta_e$ and $\beta_h$. While he could not arrive at a definite upper limit to the value of $ZT$ his theoretical studies of optimum $ZT$ vs. $\gamma$ for $E_g = 0$ showed that very high values of $ZT$ could be achieved in very small bandgap semiconductors by doping. At this point, most of the fundamental physics required to fully describe thermoelectric performance was known. Yet, most transport models were still not sophisticated enough to simultaneously include all the pertinent physics.

Significant progress was made in the fifties and the sixties towards analytically calculating the scattering parameters used in the Boltzmann transport equation. The most common modes of scattering included in the BTE were acoustic-phonon scattering through the deformation potential put forth by Bardeen and Shockley [6] and the polar-optical mode scattering put forth by Callen in 1949 [46] and Frohlich in 1954 [47]. In the case of elastic scattering such as acoustic-phonon scattering and ionized-impurity scattering, the relaxation time approach that characterizes the rate at which momentum decays can be used to solve the BTE. However in the case of inelastic scattering no relaxation time exists and hence other methods to solve the BTE were developed such as the variational calculations approach put forth by Kohler in 1948 [48], the iteration method by Rode in 1970 [49] and the matrix method by Kranzer in 1971 [50]. Meanwhile Kane in 1957 [51] determined accurately the structure of the lowest (000) conduction band minima at the center of the Brillouin zone as well as the wave functions in that valley. Using Kane's model of the bandstructure and electron wave functions, Rode [49] calculated the electron mobility in intrinsic, direct gap, polar, non-degenerate semiconductors using Maxwellian statistics. He included the three scattering mechanisms i.e. acoustic deformation potential scattering, polar optical-phonon scattering and piezoelectric scattering which he identified as the most important mode of scattering for lower lattice temperatures such as for e.g. below 60 K in GaAs. The electron distribution function under the influence of a small electric field is described as a linear finite-difference equation, which was solved using a numerical iteration method. The mobilities resulting from using parabolic vs. non-parabolic bands described by Kane were compared. Non-parabolicity affected the calculated mobility by only 10% in wide bandgap material such as GaAs while small bandgap material such as InSb showed a 50% decrease in the calculated mobility when non-parabolicity was included. Good match between the predicted and measured mobility data was seen for GaAs between the temperature ranges of 150–400 K. While the poor match with measured data at high temperatures could not be explained, the results below 150 K were attributed to the non-inclusion of impurity scattering in the model which becomes prominent at low temperatures. In 1971 Rode [52] extended the previous study to calculate mobility and thermoelectric power in degenerate direct-gap, polar semiconductors using Fermi–Dirac statistics. In addition to piezoelectric scattering, longitudinal acoustic-phonon scattering and polar optical-phonon scattering, ionized-impurity scattering and heavy hole scattering were also included in the calculations. Thermoelectric power was calculated from the short-current calculated from the perturbation distribution where the field is set equal to zero.

$$S = -\frac{\left(\frac{1}{e}\nabla\varepsilon_f + \frac{J}{\sigma}\right)}{\nabla T}. \tag{34}$$

Mobility and thermoelectric power were compared with experimental data for intrinsic InSb, InAs and InP. There was good agreement with measured mobility data for all three

semiconductors above room temperature while below room temperature the mobility showed two orders of magnitude decrease compared to experiments. Electron–hole scattering was prominent above room temperature, polar mode inelastic scattering dominated at room temperature while impurity scattering was dominant below room temperature. Below 60 K in InSb and 80 K in InAs, deformation potential acoustic mode scattering and piezoelectric scattering dominate electron mobility. Good agreement with experimental data was also seen in the case of thermoelectric power for various electron concentration levels at room temperature. However, for higher temperatures, the thermoelectric power showed slight deviation from experiments where multivalley conduction was suspected to dominate electron transport.

Mahan in 1994 [53] extended Rode's work to study the optimum bandgap in direct bandgap semiconductors. Non-parabolicity was included using the two-band Kane model and the solution to the BTE was obtained using Rode's iteration method in the Gauss–Siedel formulation because inelastic scattering was included. Comparisons were made between $ZT$ values for parabolic bands and non-parabolic bands with either elastic ionized-impurity scattering or inelastic polar optical-phonon scattering. They found that the dependence of $ZT$ on the bandgap $E_g$ fell into two regimes. For $E_g < 6k_BT$ the value of $ZT$ decreased with decreasing bandgap due to the increasing presence of minority carriers. For $E_g > 10k_BT$ the value of $ZT$ either increased or decreased depending upon the type of scattering involved. Additionally they found that the most important effect of non-parabolicity was to modify the effective mass values that in turn changed the value of the material parameter $\beta_0$ present in the expression for $ZT$ similar to the parameter $\beta$ in Chasmar and Stratton's model. Mahan determined that in order to obtain higher $ZT$ values the value of $\beta_0$ needs to increase implying that materials with higher effective masses or reduced thermal conductivity $\kappa$ needed to be researched. Table 1 summarizes the progression of thermoelectricity and the various models used for predicting thermoelectric performance since the first thermoelectric effect was discovered in 1821.

## 3.1. Development of low-dimensional models for thermoelectric applications

The concept of monocrystalline semiconductor structures having a periodic potential in one dimension was proposed by Esaki and Tsu in 1970 [54] who called these structures *superlattices*. While several low-dimensional structures can be envisaged to improve thermoelectric performance, superlattices provide a fertile conceptual testbed and have been the focus of many studies. Esake and Tsu suggested that the periodic potential could be obtained by periodic variation of alloy composition or variation of impurity density during epitaxial growth out of materials such as Si, Ge and their alloys, III–V, II–VI, compounds and their alloys etc. The dispersion relation in the direction parallel to the superlattice planes was assumed to be parabolic while in the cross-plane direction they used a sinusoidal approximation in the form of Mathieu's equation [55]

$$E\left(k_\parallel, k_\perp\right) = \frac{\hbar^2 k_\parallel^2}{2m_e^*} + t\left(1 - \cos\left(k_\perp d\right)\right) \tag{35}$$

where $d$ is the superlattice period, $k_\perp$ corresponds to the wave vectors in the cross-plane direction and $k_\parallel$ corresponds to the wave vectors in the in-plane direction of the superlattices. The amplitude of the superlattice periodic potential is given by $t$. The authors found that under moderate electric fields in the cross-plane direction the confined energy bands and wave vector zones would result in a negative conductance that could lead to new ultra-high

Table 1
Development of thermoelectric models

| | |
|---|---|
| 1821 | Seebeck effect was discovered. |
| 1834 | Peltier effect was discovered. |
| 1854 | Thomson effect was predicted and proved experimentally in 1856. |
| 1912 | Altenkirch introduced the concept of a figure of merit by suggesting that a good thermoelectric material should have large Seebeck coefficient, poor thermal conductivity to retain heat at the junctions and maintain a large thermal gradient and high electrical conductivity to minimize Joule heating. |
| 1928 | Sommerfeld presents the revised free-electron theory in metals, originally developed by Lorentz, using Fermi–Dirac statistics. |
| 1928 | Bloch shows that thermal motion of lattice and effect of impurities affect the electron mean free path leading to finite electrical conductivity. Bloch introduces the concept of conduction electrons and shows that conduction takes place only if there are unoccupied energy levels near the Fermi energy. He introduces temperature dependence of electrical conduction in metals to vary directly with $T$ and with $T^5$ for low temperatures. His theory however could not be extended to semiconductors and insulators where the electrical conductivity is very low at low temperatures. |
| 1931 | Wilson extends Bloch's theory to semiconductors and insulators with emphasis on temperature dependence of conductivity. Using the relaxation time approximation where electrons scatter with acoustic and optical phonons with energies around the Fermi energy, Wilson calculated the electrical conductivity in semiconductors and insulators to be directly proportional to $n_e m_e^{*5/2} T^{3/2}$. The direct proportionality between $\sigma$ and $n$ leads to reduced conductivities at low temperatures due to the low concentration of carriers. |
| 1931 | Sommerfeld and Frank study thermoelectric phenomena in metals based on the revised free-electron theory of metals. They obtain equations for electrical conductivity, thermal conductivity and Thomson coefficient. Local equilibrium is assumed and the number of electrons is assumed to be independent of temperature while their mean free path is assumed to be independent of velocity. |
| 1952 | Ioffe studied semiconductor thermal conductivity as a function of its atomic weight. He found that large atomic weight elements showed lower thermal conductivity that he attributed to their high density that in turn reduced the velocity of sound through these materials lowering their thermal conductivity. |
| 1953 | Johnson and Lark-Horovitz used Sommerfeld's model of electric current and thermal current to calculate thermoelectric coefficients for three separate cases as a function of temperature and impurity concentration. Seebeck coefficient calculated from Thomson coefficient using electrical and current densities. Model includes Fermi level, bandgap, temperature, ratio of electron to hole mobility and electron and hole effective masses. Low-temperature impurity scattering included by an additional correction term. Carrier-phonon scattering included as a function of temperature. In the low-temperature impurity range and transition temperature, carrier mean free path is said to be affected by the presence of impurities as a function of carrier energy in addition to electron energy independent phonon scattering. In the intrinsic temperature range, the mean free path is said to be affected only by lattice vibrations independent of carrier energy. |
| 1953 | Fredirikse modified Lark-Horovitz's model to account for low-temperature deviations from equilibrium of the lattice. The deviation from equilibrium of the lattice was found to result in a phonon current that interacts with the electron current to cause the observed deviations from the predicted thermoelectric power in germanium. |
| 1954 | Goldsmid recognized that since the electrical conductivity is affected by the crystal structure through the electron mobility, the thermoelectric properties of a material should be affected by both mobility and thermal conductivity as a function of its atomic weight. Accordingly, Goldsmid studied the ratio of the electron mobility to thermal conductivity as a function of atomic weight. Applying the selection rules of materials with high Seebeck coefficient and high atomic weight, he discovered Bismuth Telluride that provided a cooling of 26°. |

Table 1 (*continued*)

| | |
|---|---|
| 1956 | Ioffe suggested alloying semiconductors with isomorphous materials to reduce the overall thermal conductivity without affecting the electrical conductivity leading to the development of semiconducting alloy systems for thermoelectric applications. |
| 1956 | Price used Onsager's reciprocal relationships to modify Lark-Horovitz's model to include contributions from electric field, band edge energies, bandgap, low-temperature effects and phonon-drag effects. He was also the first to identify the effect of shear strain on the thermoelectric properties of materials that causes a change in the activation energies of the impurity donor atoms leading to a shift in band edge energies. |
| 1957 | Ioffe introduced $ZT$ as a means to quantify the thermoelectric performance of materials. Used simple thermodynamic considerations with Fermi–Dirac statistics in a Boltzmann-based model to calculate thermoelectric coefficients. He included the effect of electron–phonon and impurity scattering through the scattering term $r$. |
| 1959 | Chasmar and Stratton introduced the concept of a material parameter that would serve as a selection criterion for optimum thermoelectric performance. The material parameter was a function of carrier mobility, doping, effective mass, thermal conductivity and temperature. Using Ioffe's model with its scattering parameter $r$ to include various scattering effects, they were the first to identify the effect of bandgap on the figure of merit. Materials with large bandgaps were found to have low carrier mobility and high thermal conductivity. They combined their material parameter with Goldsmid's criterion of large atomic mass to identify that a combination of cadmium telluride or selenide with a selenide or telluride having small bandgap would lead to optimum performance. |
| 1961 | Littman and Davidson attempted to find an upper limit to $ZT$. They used irreversible thermodynamics to show that no upper limit exists to $ZT$. |
| 1962 | Simon studied $ZT$ in 2 band semiconductors as a function of the minimum bandgap, material parameter $\beta$ and the scattering parameter $r$. He defined another material parameter $\gamma$ that was a function of the electron and hole effective masses and their mobilities. He showed that very high $ZT$ values could be obtained in small bandgap semiconductors by doping. |
| 1971 | Rode used the iteration method to solve the BTE. This method allowed him to include inelastic scattering that was not possible through the relaxation time approximation solution to the BTE. Rode used Kane's model of the bandstructure and electron wave functions at the (000) conduction band minima at the center of the Brillouin zone to calculate the mobility and thermoelectric power of degenerate, direct bandgap polar semiconductors using Fermi–Dirac statistics. He included longitudinal acoustic-phonon scattering, polar optical-phonon scattering, piezoelectric scattering, ionized-impurity scattering and heavy hole scattering. |
| 1994 | Mahan extended Rode's work to study optimum bandgap in direct bandgap semiconductors. He found that the most important effect of non-parabolicity was to change the effective mass that in turn changed the material parameter $\beta$ and changed $ZT$. He too concluded that for high $ZT$, materials with high effective masses and low thermal conductivities needed to be researched. |

frequency oscillators. The negative conductivity will arise from the fact that electrons traveling perpendicular to the superlattice would experience negative effective mass beyond the inflection point in the sinusoidal $E$ vs. $k$ dispersion relation. In 1984 Friedman [56] suggested that the low-temperature ($k_B T < \varepsilon_f$) thermoelectric power S of a superlattice as a function of dopant concentration can be used to provide information about the one-electron density of states and the location and width of the mini-bands. Following Wilson's model for calculating thermoelectric power using Fermi–Dirac statistics in the BTE and assuming energy-independent momentum scattering rates, they showed mathematically that the thermoelectric power tends to diverge at the mini-band extrema. The divergence in S is smoothed out for energies greater than $k_B T$ but they were still discernible for low temperatures. In addition, anisotropy in the thermoelectric power was predicted for in-plane vs. cross-plane temperature gradient. For the next couple of

years the low-temperature thermoelectric power of superlattices was predominantly used as a tool to understand the electronic structure and transport properties of superlattices [57,58] as well as the scattering dynamics of electrons and phonons in solids [59,60].

In 1992, Mensah and Kangah [61] used the relaxation time approximation (RTA) model of the BTE with the sinusoidal dispersion relation for the confined direction of superlattices to obtain analytical expressions for the Seebeck coefficient and thermal conductivity of superlattices along the superlattice cross-plane direction. Defining $2\Delta$ as the width of the lowest energy mini-band in the $E$ vs. $k$ regime, the thermopower and thermal conductivity are calculated for two ranges of $\Delta$. For $\Delta \ll k_B T$, the electrons in the superlattice are said to behave as a 2D electron gas while for $\Delta \gg k_B T$ the electrons behave as a 3D gas. They suggested that by an optimal selection of $\Delta$ and $d$, the superlattice period, it is possible to obtain good-quality and efficient thermoelements. In 1993, Dresselhaus and Hicks [62] proposed that layering highly anisotropic thermoelectric materials such as $Bi_2Te_3$ alloys in the form of superlattices would make it possible to increase the figure of merit provided that the superlattice multilayers are made in a particular orientation. The model of the superlattice proposed by the authors involved layers of thin films with no barrier layers such that confinement effects originated only due to electron confinement in the thin films. They theorized that in addition to confinement effects that cause electrons to behave as a 2D gas, the layering would reduce thermal conductivity through phonon scattering and thus increase $ZT$. The layers were assumed to be parallel to the $x-y$ plane where they have a parabolic dispersion and a confined dispersion in the $z$ direction as shown in Eq. (35) which unlike the sinusoidal dispersion used in the previous papers, treats the lowest subband in the well to be flat similar to electrons confined in an infinite potential well.

$$\varepsilon\left(k_x, k_y\right) = \frac{\hbar^2 k_x^2}{2m_x^*} + \frac{\hbar^2 k_y^2}{2m_y^*} + \frac{\hbar^2 \pi^2}{2m_z^* a^2} \quad \text{where } a \text{ is the layer thickness.} \tag{36}$$

Using the dispersion relation and the equations for S, $\sigma$ and $\kappa_{el}$ and $\kappa_{ph}$ specified by Rittner [44] they calculated the figure of merit $ZT$ for transport along the $x$-axis in terms of the Fermi functions of order 1 and 0 (refer Eq. (28)) as well as the reduced Fermi energy $\varepsilon_f^*$ and a material parameter $B$ described in Eq. (37).

$$Z_{2D}T = \frac{\left(\frac{2F_1}{F_0} - \varepsilon_f^*\right) F_0}{\frac{1}{B} + 3F_2 - \frac{4F_1^2}{F_0}}$$

where

$$\varepsilon_f^* = \frac{\left(\varepsilon_f - \frac{\hbar^2 \pi^2}{2m_z^* a^2}\right)}{k_B T} \quad \text{and} \quad B = \frac{1}{2\pi a}\left(\frac{2k_B T}{\hbar^2}\right)\left(m_x m_y\right)^{1/2} \frac{k_B^2 T \mu_x}{e\kappa_{ph}}. \tag{37}$$

The authors analyzed that the value of $Z_{2D}T$ can be increased by using narrower layers that will ensure increased phonon scattering and by choosing optimum current direction and layer orientation to maximize mobility. The $Z_{2D}T$ values for $Bi_2Te_3$ were predicted for two orientations of the multilayers, the $x-y$ planes and the $x-z$ planes. The results predicted an increase in $ZT$ by a factor of 13 over the bulk value in the $x-z$ plane for current flow along the $x$-axis for layers that are $3.8\Delta$ thick. In the case of the $x-y$ plane results predicted an increase in $ZT$ by a factor of 3 over the bulk value for layers that are $10\Delta$ thick. The dispersion model used

in the above paper treats the quantum wells as decoupled such that there is no tunneling between the wells.

Sofo and Mahan [63] analyzed the $ZT$ predictions of a superlattice put forth by Hicks and Dresselhaus by incorporating alternating barrier layers having finite thermal conductivity in the superlattice and introduced a tunneling probability between the quantum wells in their calculations. They argued that quantum mixing between the wells due to tunneling leads to a broadening of the density of states from 2D to 3D. In addition, the finite thermal conductivity of the barrier region produces a parasitic effect of backflow of heat that would hinder the pumping of heat in the well. The authors used the RTA model to include electron density dependence on the electrical conductivity through the expression given by Drude [29].

$$\sigma = n_e \left( e^2 \tau / m_x \right). \tag{38}$$

The dependence of the electrical conductivity on electron density ensures that if the well width $a$ and chemical potential $\varepsilon_f$ are kept constant, just by increasing the barrier width $b$, the electron density will decrease due to reduced tunneling probability causing the electrical conductivity to decrease and decrease $ZT$. Alternately, for a fixed barrier width, as the well width is reduced, the 2D density of states increases and proportionately increases the electrical conductivity as well as $ZT$. The thermal conductivity equation was also modified to include heat backflow at the barriers in the thermal conductivity. In addition they changed the value of $B$ to be inversely proportional to the superlattice period $d$ and not the well thickness $a$. Sofo and Mahan used their model to predict the $ZT$ vs. well width values for $Bi_2Te_3$ layers in the $x-y$ plane with transport along the $x$-axis. Using average values in the literature for the mobility $\mu_x$ and thermal conductivity $\kappa$, they found that there was improvement in $ZT$ due to the enhancement of density of states at the bottom of the lowest subband with decreasing well width but the amount of increase was not as high as originally predicted by Dresselhaus and Hicks. The change in $ZT$ with decreasing well width was studied as a function of the barrier width. In all cases except for a $20\Delta$ wide barrier the $ZT$ values increase with decreasing well thickness. The decrease in $ZT$ for the $20\Delta$ barrier was attributed to tunneling through the barrier that causes quantum coupling between the wells leading to broadening of density of states making the 2D density of states to become 3D density of states and reduce $ZT$. The authors also point out that the flat subband assumption works well when the Fermi level lies above the subband at a distance greater than the value of $k_B T$ as electrons above and below the Fermi level have opposite contribution to the thermopower. Similar studies on the effect of tunneling and finite thermal conductivity contribution of the barrier material were done by Broido and Reinecke [64] in 1995 who studied the effects of confinement on the figure of merit of $Bi_2Te_3$ superlattices using Kronig–Penny type subband energy dispersion in the RTA model. They too found that the value of $ZT_{2D}$ increased as the well width decreased until tunneling between wells caused the value of $ZT_{2D}$ to reduce for further decrease in well width.

In 2001 Broido and Reinecke [65] extended the BTE model with Kronig–Penny subbands to calculate thermoelectric coefficients in quantum well and quantum wire superlattices. The thermoelectric coefficients were calculated for the occupied subbands in each conduction band valley neglecting inter-valley scattering. The results for each valley were summed over all the multiple ellipsoidal conduction band valleys to obtain the overall thermoelectric coefficients. Elastic acoustic-phonon scattering through the deformation potential scattering and inelastic optical-phonon scattering using the solution to the inelastic 3D Boltzmann transport equation were included in the calculations. Optical phonons were assumed to be dispersionless with the dominant

phonon energy to be the value of its zone center $\hbar\omega_0$. The BTE solution for inelastic scattering was obtained by using an extension of Ritz's iterative method [66]. The thermoelectric coefficients were compared to the results of the constant relaxation time approximation (CRTA) and bulk values as a function of decreasing well width. In general, solutions based on the CRTA were found to predict much higher values for mobility compared to the inelastic solution. Power factor predictions made by both CRTA and inelastic scattering methods predicted lower values than the bulk which were attributed to electron confinement in the wells leading to reduced conductivity. The power factor values increased with decreasing well width due to increase in the 2D density of states and eventually matched the bulk power factor. However, further decrease led to electron tunneling that changed the 2D density of states to 3D lowering the power factor. These effects as seen previously were not captured by the CRTA model. The effect of scattering and bandstructure on the thermoelectric performance was demonstrated through the power factor studies done on two materials, PbTe and GaAs. PbTe has an anisotropic multivalley bandstructure while GaAs has a single isotropic conduction band valley. At room temperature both acoustic-phonon and optical-phonon scattering dominate in PbTe while only optical-phonon scattering dominates in GaAs. Accordingly the full solution of the BTE including elastic acoustic-phonon and inelastic optical-phonon scattering showed an increase of only a factor of two in the power factor of PbTe compared to its bulk value while GaAs showed a factor of 9.5 increase in its power factor.

The ability to incorporate the full bandstructure information to calculate the thermoelectric coefficients was demonstrated by Sofo et al. in 2003 [67] when they presented a method of calculating the electronic structure from first principle calculations, which they included in the relaxation time approximation to calculate the transport coefficients. They defined a kernel of all transport coefficients known as the *transport distribution* that contains all the electronic information needed to obtain the thermoelectric coefficients directly for any given material as shown in Eq. (39).

$$S = \frac{ek_B}{\sigma} \int d\varepsilon \left( -\frac{\partial f_0}{\partial \varepsilon} \right) \Xi(\varepsilon) \frac{\varepsilon - \mu}{k_B T} \quad \text{where } \Xi = \sum_{\vec{k}} \vec{v}_{\vec{k}} \vec{v}_{\vec{k}} \vec{\tau}_{\vec{k}}. \tag{39}$$

The group velocity values are obtained using the linear augmented plane wave (LAPW) method while the relaxation times are calculated for various scattering mechanisms using parameters found in the literature. Doping was included by changing the relative position of the Fermi level under the assumption that the bandstructure remains unchanged as the Fermi level changes. The above method was used to calculate the thermoelectric coefficients for $Bi_2Te_3$ using experimentally determined thermal conductivity values for the various planes. The Seebeck coefficient for all doping levels was calculated using a constant relaxation time that gave the best fit with experimental data in the intrinsic region. For all doping levels, the Seebeck coefficient of the n-type material showed a better fit with experiments compared to the p-type. The model also captured effectively the anisotropy in the electrical conductivity of $Bi_2Te_3$ where the conductivity along the basal plane can be four times greater than the conductivity along the trigonal axis. The predictions for the figure of merit however did not show very good match with experiments with results for the n-type matching better than those for the p-type. Similar match with experimental data was obtained by Lee and Allmen in 2006 [68] who calculated the thermoelectric coefficients using a tight-binding model with $sp^3d^5s^*$ orbitals, nearest neighbor interactions and spin–orbit coupling for $Bi_2Te_3$ in the constant relaxation time approximation model. Table 2 summarizes the progression of models used for predicting thermoelectric performance in low-dimensional structures.

Table 2
Low-dimensional thermoelectric models

| | |
|---|---|
| 1970 | Esaki and Tsu introduced superlattice structures for applications as ultra-high-frequency oscillators. Using a sinusoidal approximation to the dispersion relation in the confined direction, they showed that the confined energy bands and wave vector zones would lead to negative conductance that could lead to ultra-high frequency oscillators. |
| 1984 | Friedman recognized that low-temperature thermoelectric power of superlattices as a function of doping would reveal information about the density of states and width of the mini-bands. He was also the first to predict the anisotropy of the Seebeck coefficient between the in-plane and cross-plane directions. |
| 1992 | Mensah and Kangah used the RTA model with the sinusoidal dispersion approximation to obtain analytical expressions for the Seebeck coefficient and thermal conductivity of superlattices treating the electrons in the superlattice to behave as a 2D or 3D electron gas depending on the width of the lowest energy mini-band. |
| 1993 | Dresselhaus and Hicks proposed that layering highly anisotropic thermoelectric materials in the form of superlattices would increase the figure of merit in a particular orientation as the thermal conductivity in that direction would decrease due to phonon scattering. The orientation would be chosen based on optimum current direction and maximum mobility. Dresselhaus and Hicks used 2D density of states for a superlattice film in the BTE model with Fermi–Dirac statistics to calculate the thermoelectric coefficients. |
| 1994 | Sofo and Mahan modified Dresselhaus and Hicks calculations to incorporate alternating barrier layers of superlattices with finite thermal conductivity as well as a tunneling probability between the quantum wells. They argued that quantum mixing between the wells changes the density of states from 2D to 3D. In addition, the finite thermal conductivity of the barrier layers would introduce a parasitic backflow of heat that would hinder the pumping of heat in the well. Accordingly, the predicted improvement in $ZT$ was not as high as predicted by Dresselhaus and Hicks. Sofo and Mahan studied the effect of well and barrier width on the figure of merit for optimum thermoelectric performance. They showed that thermoelectric performance increased as a function of decreasing well width until tunneling between the wells changed the 2D density of states to 3D leading to decrease in $ZT$. |
| 1995 | Broido and Reinecke extended the BTE model to calculate thermoelectric coefficients in quantum well and quantum wire superlattices using the Kronig–Penny model for subbands and used their model to validate the results predicted by Sofo and Mahan in 1994. |
| 2001 | Broido and Reinecke extended their model to include acoustic deformation-potential-based elastic phonon scattering and inelastic optical-phonon scattering using the inelastic 3D BTE solution using an extension of Ritz's iterative method. The thermoelectric coefficients were calculated and compared to the results of the constant relaxation time approximation (CRTA) model. It was shown that in general the CRTA model tends to predict higher values of mobility compared to the inelastic scattering methods leading to higher electrical conductivity and hence higher power factor predictions. They also acknowledged that predicted power factor values were lower than the bulk values due to electron confinement. |
| 2003 | Sofo et al. incorporated the full bandstructure to calculate the thermoelectric coefficients using the constant relaxation time approximation model. Experimentally determined thermal conductivity was used and the constant relaxation time was obtained using the value that gave the best fit for the predicted Seebeck coefficient with experimental data. Doping was included by changing the relative position of the Fermi level assuming no change in bandstructure. The model captured the anisotropy of electrical conductivity in $Bi_2Te_3$ but overall figure of merit predicts did not show a good match with experiments. |
| 2005 | Bulusu and Walker used the non-equilibrium Green's function method to study the thermoelectric performance of silicon nanofilms, nanowires and Si/Ge/Si superlattices. Quantum effects were modeled through the dispersion relation for each subband. Electrons were modeled to undergo inelastic inter-valley scattering with optical phonons. The effect of confinement and scattering on the electrical conductivity and Seebeck coefficient were studied in addition to the effect of substrate strain, in the case of quantum well superlattices. |

## 3.2. Nanostructured thermoelectric materials

The advent of quantum well nanofilm and nanowire superlattice structures that improve the value of *ZT* due to a number of advantages has shifted the focus towards understanding

carrier transport behavior in nanostructures. Quantum confinement in nanostructures increases the local carrier density of states per unit volume near the Fermi energy increasing the Seebeck coefficient [62] while the thermal conductivity can be decreased due to phonon confinement [69, 70] and phonon scattering at the material interfaces in the superlattices [62,71,72]. Normally, the electrical conductivity is assumed *not* to be significantly affected due to the large semiconductor bandgap and the disparity between the electron and phonon mean free paths [25,73]. This assumption is also a consequence of the predominantly particle-based models. The combined benefits of reduced thermal conductivity and improved Seebeck coefficient imply a theoretically higher *ZT* compared to the bulk structures. However, experimental observations have not been able to achieve the presumed benefits of superlattice thermoelectric devices despite theoretically predicted improvements in *ZT* and experimentally observed reduction in the thermal conductivity of superlattices compared to their bulk counterparts [74,75]. Hence there is a need to better understand the effect of all the significant factors contributing to the thermoelectric figure of merit of nanoscale devices. In this regard, the two main phenomena that affect electron transport in nanostructures are (1) electron confinement and (2) electron scattering effects such as electron–phonon scattering, electron–impurity scattering etc.

Shrinking device dimensions presents an increasing need for a quantum transport model that can effectively couple scattering effects. The need to incorporate scattering stems from the fact that while electron–phonon scattering usually helps restore thermodynamic equilibrium, shrinking device dimensions may not ensure enough scattering to restore equilibrium. The simultaneous consideration of scattering effects, which is usually described as particle behavior, and quantum effects, which are wave in nature, is confounding and computationally intensive. In this regard the non-equilibrium Green's function formalism provides a framework for coupling quantum effects and thermal effects to model electron transport in thermoelectric devices. Open boundary conditions allow the source and drain contacts to be coupled to the device through simple self-energy terms. In addition, the NEGF formalism *does not* require a statistical distribution of carriers within the device thus allowing for the rigorous incorporation of both elastic and inelastic scattering effects using the concept of Buttiker probes [76]. A brief synopsis of the formalism is presented here while a more thorough and detailed development can be found in [76] and [77]. The first reported use of NEGF to predict thermoelectric performance is found in [78–80]. True quantum simulations have to see widespread use, but modern devices demand this level of modeling.

## 4. The NEGF formalism

In general an isolated device and its energy levels are described using a Hamiltonian $H$, a Hartree potential $U$ and energy eigenstates of the electron, $\varepsilon_\alpha$.

$$(H + U)\, \psi_\alpha(\vec{r}) = \varepsilon_\alpha \psi_\alpha(\vec{r}). \tag{40}$$

The potential $U$ is obtained using Poisson's equation and accounts for the effect of any change in the density matrix on the channel capacitance. The channel capacitance consists of an electrostatic capacitance that depends on the dielectric constant $\varepsilon_r$ and a quantum capacitance, which depends on the density of eigenstates in the channel [77]. In general, the electron density matrix in real space is given by

$$\left[ \rho(\vec{r}, \vec{r'}; \varepsilon) \right] = \int_{-\infty}^{+\infty} f\left( \varepsilon - \varepsilon_f \right) \delta\left( [\varepsilon I - H] \right) d\varepsilon. \tag{41}$$
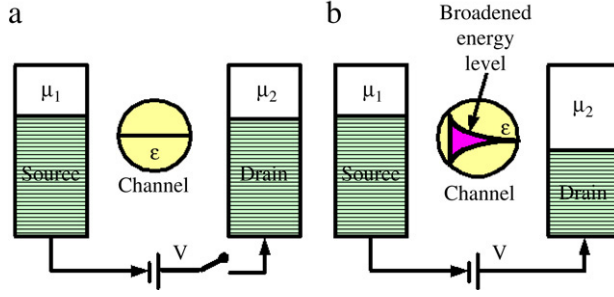
Fig. 3. (a) Single energy level of an isolated channel (b) Broadening of electron energy levels in the channel when connected to contacts.

Here $\delta(\varepsilon I - H)$ is the local electronic density of states given as

$$\delta\left(\varepsilon I - H\right) = \frac{\mathrm{i}}{2\pi}\left[G(\varepsilon) - G^{+}(\varepsilon)\right] \quad \text{where } G(\varepsilon) = [(\varepsilon - \mathrm{i}0^{+})I - H]^{-1}. \tag{42}$$

$G(\varepsilon)$ is the retarded Green's function while $G^{+}(\varepsilon)$, its conjugate complex transpose, is called the advanced Green's function. In the time domain, the Green's function can be interpreted as the impulse response of the Schrödinger equation where in the present scenario the impulse is essentially an incoming electron at a particular energy. In the energy domain the Green's function gives the energy eigenvalues for the eigenstates that are occupied in response to the applied impulse. The diagonal elements of the spectral function, which is the difference between the retarded and advanced Green's function, represent the available local electron density of states.

When an isolated device is connected to source and drain contacts, the difference in the Fermi levels of the source and drain causes electrons to flow from the source to the drain through the channel. The distribution of electrons in the semi-infinite source and drain is said to follow the Fermi distribution with $\varepsilon_{f1}$ and $\varepsilon_{f2}$ the chemical potentials of the source and the drain and $f_1$ and $f_2$ their Fermi functions. When no scattering is incorporated in the channel, transport is ballistic in nature and is expected to have zero resistance to current flow. However, experimental measurements [81] have shown that the maximum measured conductance of a *one-energy* level channel approaches a limiting value $G_0 = 2e^2/\hbar = 51.6(\mathrm{k}\Omega) - 1$. The reason for this limit to conductance arises from the fact that current in the contacts is carried by infinite transverse modes while the number of available modes for a one-energy level channel is very limited. When the channel consisting of a single energy level $\varepsilon$ is connected to the contacts current can flow only when $\varepsilon$ lies between $\varepsilon_{f1}$ and $\varepsilon_{f2}$ ($\varepsilon_{f1} > \varepsilon > \varepsilon_{f2}$). Once the value of $\varepsilon$ is ensured to lie near $\varepsilon_{f1}$ some of the density of states from the source spread into the channel causing broadening of the available density of states around $\varepsilon$ as seen in Fig. 3. There will be some broadening of energy levels around the drain as well but if the difference between $\varepsilon$ and $\varepsilon_{f2}$ is large, the broadening will be very small and only few states will become available near the drain to remove the electrons coming from the channel. As the applied bias is increased linearly, more and more states between $\varepsilon$ and $\varepsilon_{f2}$ become available to remove electrons from the channel causing the source to increase its supply of electrons into the channel. This phenomenon results in a linear increase of current in the channel. When the applied bias reaches a high enough value such that no additional states open up in the drain, the number of available density of states remains constant at the energy level $\varepsilon$ and the channel current reaches saturation and the current will not increase any further. The above analogy of a one-energy level system is applicable to nanoscale thin films and wires

where available energy levels along the confined dimension are very limited in addition to being spaced far apart from adjacent energy levels.

In the NEGF formalism the coupling of the device to the source and drain contacts is described using self-energy matrices $\Sigma_1$ and $\Sigma_2$. The self-energy term can be viewed as a modification to the Hamiltonian to incorporate the boundary conditions. Accordingly, Eq. (40) can be rewritten as

$$\left( H + U + \sum_1 + \sum_2 \right) \psi_\alpha (\vec{r}) = \varepsilon_\alpha \psi_\alpha(\vec{r}). \tag{43}$$

The self-energy terms $\Sigma_1$ and $\Sigma_2$ originate from the solution of the contact Hamiltonian. In this semi-infinite system, which is connected to the channel, there will be an incident wave from the channel as well as a reflected wave from the contact. The wave function at the interface is matched to conserve energy resulting in the boundary condition,

$$\sum_j = -t \exp(\mathrm{i} k_j a) \tag{44}$$

where $a$ is the grid spacing and $t$, the inter-unit coupling energy resulting from the discretization is given by

$$t = \frac{\hbar^2}{2m^* a^2}. \tag{45}$$

The broadening of the energy levels introduced by connecting the device to the source and drain contacts is incorporated through the Gamma functions at each contact given by

$$\Gamma_j = \mathrm{i} \left( \sum_j - \sum_j^+ \right). \tag{46}$$

The self-energy terms affect the Hamiltonian in two ways. The real part of the self-energy term shifts the device eigenstates or energy level while the imaginary part of $\Sigma$ causes the density of states to broaden while giving the eigenstates a finite lifetime. The electron density for the open system is now given by

$$[\rho] = \int_{-\infty}^{+\infty} \left[ G(\varepsilon) \overset{in}{\sum}(\varepsilon) G^+(\varepsilon) \right] \left( \frac{\mathrm{d}\varepsilon}{2\pi} \right) \tag{47}$$

where

$$\left[ \overset{in}{\sum}(\varepsilon) \right] = [\Gamma_1(\varepsilon)] f_1 + [\Gamma_2(\varepsilon)] f_2. \tag{48}$$

The real portion of the diagonal elements of the density matrix, represent the electron density distribution in the channel. This electron density represented as $n$ is used in the Poisson's equation to self-consistently solve for the potential in the channel where $N_d$ is the donor density and $\varepsilon_r$ is the permittivity of the channel.

$$\nabla^2 U = -\frac{e}{\varepsilon_r} (N_d - n_e). \tag{49}$$

For plane wave basis functions, the current through the channel is calculated as the difference between the inflow and the outflow at any given contact.

$$I_j = -\frac{e}{\hbar} \int_{-\infty}^{\infty} \text{trace}\left[\Gamma_j A\right] f_j - \text{trace}\left[\Gamma_j G^n\right] \tag{50}$$

where the subscript $j$ indexes the contacts. $A$ represents the electron density of states matrix while $G^n$ is the channel electron density matrix. For a two-terminal device $I_1 = -I_2$.

## 4.1. Incorporating electron scattering in the NEGF

In addition to the source and drain contacts electrons can scatter into and out of the channel by either phonon absorption or phonon emission such that $\varepsilon_n - \varepsilon_m = \hbar\omega$. The transition of the electrons from $\varepsilon_n$ to $\varepsilon_m$ and vice versa is dependent on the transition rate $S(k, k')$ which is obtained using Fermi's Golden Rule [81]. This coupling can be expressed through a broadening term $\Gamma$ which is related to the transition rate $S$ as

$$\frac{\Gamma}{\hbar} = S\left(k, k'\right) \quad \text{where } \Gamma_{nn} = 2\pi \left|K_{mn}^{em}\right|^2 (N_\omega + 1)\, \delta\left(\varepsilon_n - \varepsilon_m - \hbar\omega\right)$$

$$+ 2\pi \left|K_{mn}^{ab}\right|^2 (N_\omega)\, \delta(\varepsilon_n - \varepsilon_m + \hbar\omega). \tag{51}$$

The broadening term obtained through Fermi's Golden Rule is similar to the broadening term in the NEGF which is expressed as

$$\Gamma_s = \int \frac{\mathrm{d}\,(\hbar\omega)}{2\pi} \left[ \begin{matrix} S_o^{em}\,(N_\omega + 1)\left[G^P\,(\varepsilon - \hbar\omega) + G^n\,(\varepsilon + \hbar\omega)\right] \\ +S_o^{ab}\,(N_\omega)\left[G^n\,(\varepsilon - \hbar\omega) + G^P\,(\varepsilon + \hbar\omega)\right] \end{matrix} \right]. \tag{52}$$

$G^n(\varepsilon)$ is the electronic density of states and $G^P(\varepsilon)$ is the hole density of states and correspond to the $\delta(\varepsilon_n - \varepsilon_m \pm \hbar\omega)$ terms while $S_o$ corresponds to the value $|K_{mn}|^2$, terms for emission and absorption of phonons in Eq. (52). For the case where electrons in the channel scatter with a phonon of single frequency, the broadening term can be simplified to

$$\Gamma_s = S_o \left[ \begin{matrix} (N_\omega + 1)\left[G^P\,(\varepsilon - \hbar\omega) + G^n\,(\varepsilon + \hbar\omega)\right] + \\ N_\omega\left[G^n\,(\varepsilon - \hbar\omega) + G^P\,(\varepsilon + \hbar\omega)\right] \end{matrix} \right]. \tag{53}$$

Since the imaginary part of the self-energy term is responsible for broadening, the scattering self-energy $\sum_s$ can be expressed using Eq. (54) as

$$\sum_s = -\mathrm{i}\frac{\Gamma_s}{2}. \tag{54}$$

The value of $S_o$ for a single phonon of energy $\hbar\omega_o$ is obtained as a sum over all phonon wave vectors $\xi$ in the Brillouin zone as

$$S_o = \sum_\xi \frac{D_o^2\,\hbar^2}{2\rho_m\,\Omega\,(\hbar\omega_o)} = \frac{D_o^2\,\hbar^2}{12\pi^2\rho_m\,(\hbar\omega_o)} \left(\frac{\pi}{a}\right)^3 \tag{55}$$

$\rho_m$ is the mass density, $\omega_o$ the phonon frequency and $D_o$ is the optical deformation potential and $a$, the lattice constant. An example of single-phonon scattering is $g$-type inter-valley longitudinal optical-phonon scattering of electrons from the [001] valley into the [00$\bar{1}$] valley in silicon [82].

The scattering self-energy is included in the Green's function seen in Eq. (56) as an additional contact that scatters electrons into and out of the channel such that the net current through the scattering contact is zero.

$$G(\varepsilon) = \left[ \left( \varepsilon - \mathrm{i}0^+ \right) I - H - \sum_1 - \sum_2 - \sum_s \right]^{-1}. \tag{56}$$

### 4.2. Calculating subband currents

The electrons in a 2D film can be treated as having infinite range of energies along the $x$- and $y$-axis while being confined along the $z$-axis which is also the direction of transport.

$$\varepsilon(k) = E_c + \frac{\hbar^2 k_x^2}{2m_x^*} + \frac{\hbar^2 k_y^2}{2m_y^*} + \frac{\hbar^2}{2m_z^*} \left( \frac{n\pi}{L_z} \right)^2 \quad \text{where } n = 1, 2, 3 \dots. \tag{57}$$

The term $k_z = n\pi/L_z$ is the wave vector corresponding to the confined electrons that form discrete standing waves when confined in an infinite potential well and $n$ is the subband index. For the film we use a 2D Fermi function given in Eq. (58) that accounts for the infinite states along the $x$–$y$ plane.

$$f_{2D}(\varepsilon) = N_0 \log \left( 1 + \exp \left( -\frac{\varepsilon - \varepsilon_f}{k_B T} \right) \right) \quad \text{where } N_0 = \frac{m_e^* k_B T}{2\pi \hbar^2}. \tag{58}$$

For transport along the $z$-direction, the electron energy is written as

$$\varepsilon(k) = E_c + \frac{\hbar^2}{2m_z^*} \left( \frac{n\pi}{L_z} \right)^2. \tag{59}$$

In the NEGF formalism, the energy of each subband is obtained directly by solving for the eigenvalues of the Hamiltonian [$H$]. The conduction band and subsequent subbands are treated as individual, single-energy channels. In the case of ballistic transport where there is no scattering between energy levels, this approach allows us to model electron transport in the device separately for each energy level. Accordingly, current–voltage characteristics are obtained for the conduction band and each additional subband separately. The current thus obtained is summed over all the bands to obtain the net channel current. We start by writing the Schrödinger wave equation along the $z$-axis as

$$[H] \psi_{nz} = \varepsilon_{nz} \psi_{nz}. \tag{60}$$

The electron energies along the $z$-axis can be obtained by substituting a plane wave basis for the electron wave function in the Hamiltonian and solving the Schrödinger wave equation along the $z$-axis using the finite-difference method.

$$\varepsilon_n(k_z) = E_c + 2t \left( 1 - \cos \left( k_{nz} a \right) \right). \tag{61}$$

When solved in this way, the value of $k_z$ for an isolated channel will be equal to $n\pi/L_z$ corresponding to standing waves in the channel. When the channel is connected to the contacts, the wave vectors associated with the broadened energy levels around each band can be obtained by solving the energy conservation equation. For example, the wave vectors corresponding to the
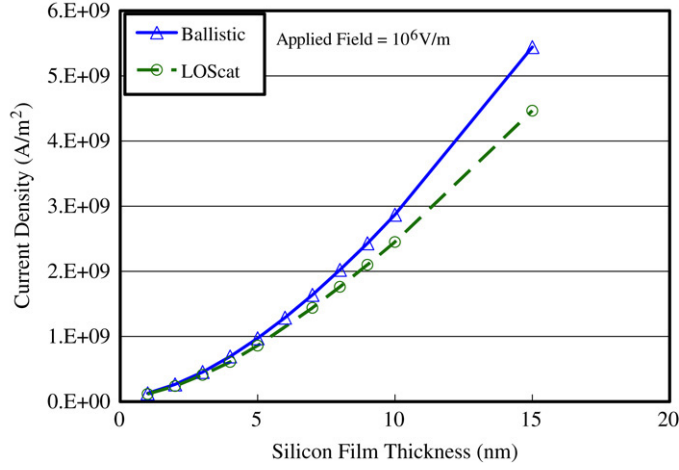
Fig. 4. Current density vs. thickness of silicon film doped to $10^{18}$ cm$^{-3}$ for (a) ballistic electron transport and (b) electron transport with longitudinal optical-phonon scattering.

broadened energy states around the conduction band $E_c$ are

$$k_z a = \cos^{-1}\left[1 - \frac{\varepsilon - E_c}{2t}\right]. \tag{62}$$

Similarly, wave vectors for broadened states around the first subband are obtained as

$$k_z a = \cos^{-1}\left[1 - \frac{\varepsilon - E_{\text{sub1}}}{2t}\right] \quad \text{and so on.} \tag{63}$$

For each energy band, the channel current–voltage characteristics are obtained independently until the contribution by any additional subbands is negligible. The final channel current at a particular voltage is obtained as the sum of the currents of the conduction band and the contributing subbands.

## 5. Comparison of models

### 5.1. Effect of electron confinement and electron–phonon scattering in silicon films

The NEGF method is used to calculate the current density for varying thickness of a silicon film for a constant applied field of $10^6$ V/m as shown in Fig. 4. The current density is obtained for two cases (1) ballistic electron transport through the film and (2) electrons undergoing inter-valley scattering with longitudinal optical phonons. The values of the various constants used in our simulations are listed in Table 3. Three important effects are demonstrated in Fig. 4. The current is very small for small film thicknesses and increases as the film thickness increases. This is the effect of electron confinement where the very small film leads to discrete subband energies that are spaced far apart in the energy space of the Brillouin zone. The electrons in thin films have very limited number of subbands available for transport leading to low current density. The second important effect is the impact of longitudinal electron–phonon scattering on the current density. Since very small films have limited states available for electron transport, electrons cannot easily scatter into or out of the subbands spaced far apart from each other. As a result, the
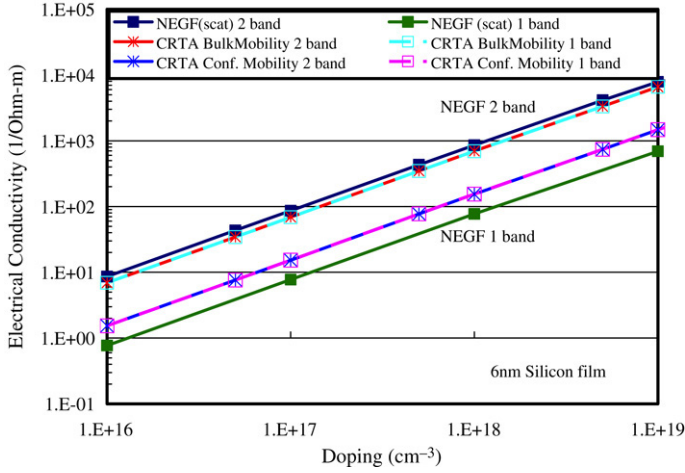
Fig. 5. Comparison of the electrical conductivity predictions between the NEGF model and the CRTA model [75,83] for a 6 nm silicon film.

Table 3
Material parameters used in the NEGF model

| | |
|---|---|
| Effective mass of silicon | $0.91m_e$ |
| Effective mass of germanium | $0.95m_e$ |
| Grid spacing $a$ | 2 A |
| Fermi energy | 0.1 eV |
| Relative permittivity of silicon | 11.7 |
| Relative permittivity of germanium | 16 |

effect of scattering is very small for film thicknesses below 5 nm. As the film thickness increases, the subband energies are spaced closer to each other and are also lower in energy as they come closer to the conduction band edge. As a result the effect of scattering becomes significant for film thicknesses greater than 5 nm where the decrease in current is now 10% of the ballistic current. The limited impact of scattering on the current demonstrates the third important effect i.e. the non-equilibrium nature of electron transport in silicon films with thicknesses equal to or less than 5–7 nm. Scattering with phonons is a way of restoring equilibrium in a system. If the electrons experience very limited scattering with phonons, they are in a state of non-equilibrium and Fermi–Dirac statistics may no longer be applicable to describe electron distribution.

In Fig. 5, the conductivity predictions from the NEGF model for 6 nm and 12 nm silicon films are compared to the electrical conductivity predicted using the constant relaxation time approximation (CRTA) model [75,83] discussed in Section 3.1, similar to the NEGF model. For electrical conductivity calculations, the CRTA model requires the value of mobility $\mu$ in the direction of transport shown in Eq. (64). $F_0$ is the Fermi integral of order 0 (refer Eq. (28)).

$$\sigma = \frac{1}{2\pi a} \left( \frac{2k_B T}{\hbar^2} \right) \left( m_x m_y \right)^{1/2} F_0 e \mu. \qquad (64)$$

Because of the conflict in the electron mobility behavior with decreasing film thickness seen in the literature [84–87], we use the bulk mobility value of silicon as a benchmark for calculating the electrical conductivity using the CRTA model.
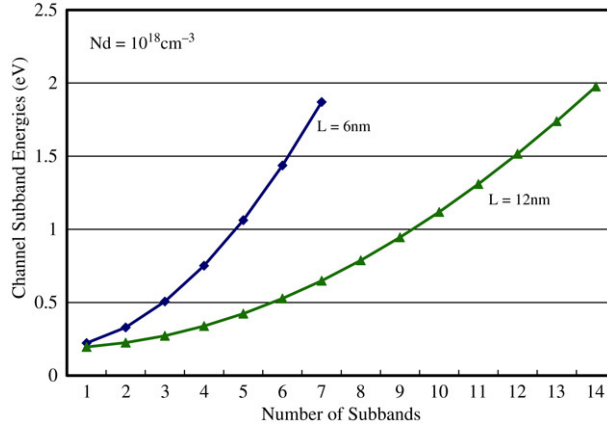
Fig. 6. Subband energies of 6 nm and 12 nm silicon films for a doping of $10^{18}$ cm$^{-3}$.

The conductivity predicted by the CRTA model for a single subband and the conductivity summed over two subband energies were found to be the same for a 6 nm film while the NEGF model predicts a 95% difference between the two cases. The number of subbands chosen was based on the proximity of the subband energy levels to the conduction band similar to data shown in Fig. 6 for the case of $10^{18}$ cm$^{-3}$ doping. Similarly, in the case of the 12 nm film, the conductivity predicted by the CRTA model for a single band differed from the conductivity summed over 6 subbands by 16%–32% for a doping range of $10^{16}$ to $10^{20}$ cm$^{-3}$. Since the conductivity predictions of the CRTA model are directly proportional to the mobility, a value of 300 cm$^2$/V s, corresponding to the mobility of a 20 nm silicon film [84] instead of bulk mobility resulted in a 77% decrease in the conductivity predicted by the CRTA model. The results indicate that for a given mobility, the effect of confinement is captured in part by the CRTA model when confined dispersion is used. The effect of electron confinement in the CRTA model predominantly comes from the value of mobility used which has to be determined experimentally or through additional quantum correction terms [88–90]. Fig. 5 reiterates the fact that quantum effects are not inherent in Boltzmann models. While approximations to the Boltzmann model may work to a certain degree, they may not be able to cope with the advances being made in nanostructural devices. The NEGF method with its ability to couple scattering effects in a quantum model provides the key to this problem.

## 5.2. Thermoelectric properties of Si/Ge/Si quantum well superlattices

Green's function approach is used to study the cross-plane thermoelectric properties of Si/Ge/Si quantum well superlattices with varying film thicknesses. Cross-plane transport is interesting because thermal conductivity can be reduced by a factor of 5–6 compared to the in-plane direction [91]. As seen from the previous section electron–phonon scattering starts to affect transport in silicon films with thicknesses of 5nm and higher. Since silicon and germanium have the same crystalline structure and the film thickness considered in this paper range from 1–3 nm, electron transport is modeled as purely ballistic.

The superlattice considered in this analysis is modeled as a 1D grid with a spacing of $a$ and the number of grid points $N$, such that the silicon film thickness is given by $L_{Si} = a(N_{Si} - 1)$. The thickness of germanium film is $L_{Ge} = a(N_{Ge} - 1)$. As the thickness of each layer changes the
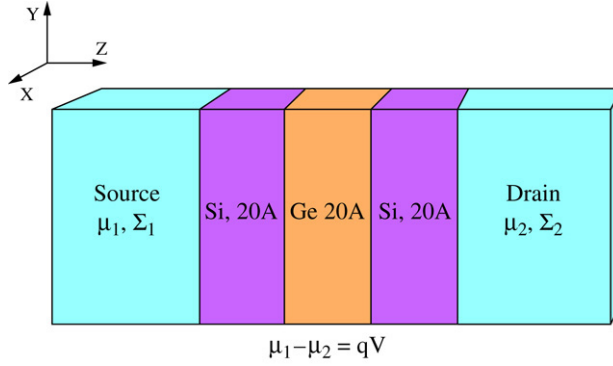
Fig. 7. Structure of the Si/Ge/Si superlattice modeled in this paper.

grid spacing is determined to ensure that the value of $t$ (Eq. (45)) is always greater than the energy range of integration above the conduction band [77]. As seen from Fig. 7, electron transport is modeled in the cross-plane $z$ direction of the superlattice, which is also the confined direction, with an effective mass Hamiltonian in that direction. The various material parameters used in the NEGF calculation are shown in Table 1. The integration range for electron energy is from $-1$ to 1 eV over 1200 integration steps. The integration step size and lattice spacing were adjusted to ensure that convergence and grid independence were obtained. For a constant doping level in the superlattice, the silicon layers due to their higher bandgap form a barrier to transport while the germanium layers form the potential well. Doping in the NEGF model is applied using Eq. (65) by varying the relative difference between the Fermi level and conduction band edge [92].

$$N_d = N_c \exp\left(-\frac{(E_c - \varepsilon_f)}{k_B T}\right). \tag{65}$$

The Seebeck coefficient for the superlattice is calculated by applying a temperature gradient along the $z$-axis. This is achieved by keeping the source temperature constant at 300 K while changing the temperature in the drain Fermi function (shown in Eq. (58)) in increments of 10 from 300–330 K. The applied bias ranges from 0 to 0.05 V. At low bias conditions, the higher temperature at the drain results in diffusion of electrons from the drain towards the source, opposing the direction of the bias leading to negative current values. As the applied bias is increased, more electrons from the source drift towards the drain and at a particular voltage, which we call the Seebeck voltage; the diffusion of electrons from the drain to the source is balanced by the drift current from the source to the drain leading to zero current. The Seebeck voltage obtained for each temperature gradient is divided by the temperature difference to obtain the Seebeck coefficient. The current–voltage characteristics are calculated for the conduction band and 10 contributing subbands.

Fig. 8 shows the predicted Seebeck coefficient vs. doping of Si/Ge/Si superlattices for varying thicknesses of the superlattice layers. The predicted Seebeck values are compared to experimental measurements taken from Refs. [74,93–95]. The experimental values for the Seebeck coefficient were measured for a wide range of temperatures while the values used here are an average for the temperature range of 300–330 K. It can be seen from Fig. 8 that there is no significant change in the Seebeck coefficient for the superlattices with the silicon 2 nm layers. Only the superlattice with the silicon 3nm layer shows a Seebeck coefficient that is higher
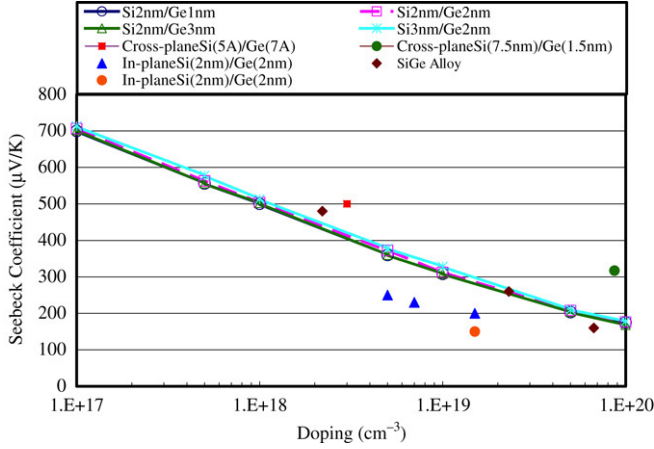
Fig. 8. Seebeck coefficient of Si/Ge/Si superlattices calculated using the NEGF model compared to experiments [74, 93–95].
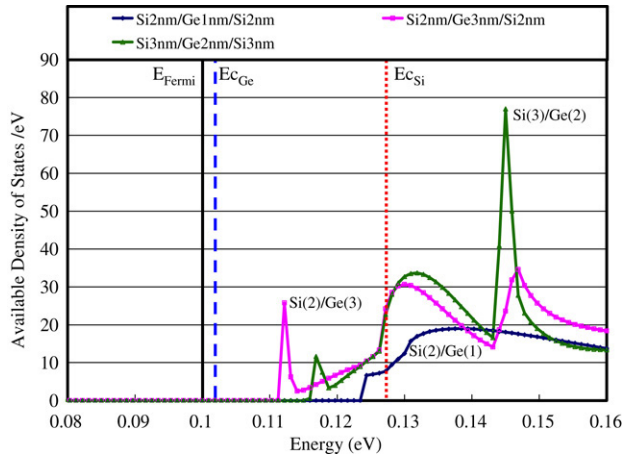


Fig. 9. Available density of states vs. energy for Si/Ge/Si superlattices with varying thickness. Silicon and germanium are doped to $Nd = 10^{19}$ cm$^{-3}$. The reference Fermi energy is 0.1 eV for both materials.

by approximately 20 μV/K. This behavior can be understood from Fig. 9 where the available densities of states at the Seebeck voltage for three different superlattices are plotted as a function of the electron energy. The energy range chosen corresponds to the energy levels that contribute to transport in the superlattice. The conduction band edges for silicon and germanium are plotted as dashed lines.

It is seen from Fig. 9 that the majority of electrons contributing to transport in the Si(3 nm)/Ge(2 nm) superlattice have energy that lies above the conduction band in silicon. The energy of these contributing levels is also slightly higher than the energy levels contributing to transport in the Si(2 nm)/Ge(1 nm) and Si(2 nm)/Ge(3 nm) superlattices. As a result the Seebeck voltage developed in the Si(3 nm)/Ge(2 nm) superlattice will be higher as a higher field is required to balance the diffusion of the high energy electrons.
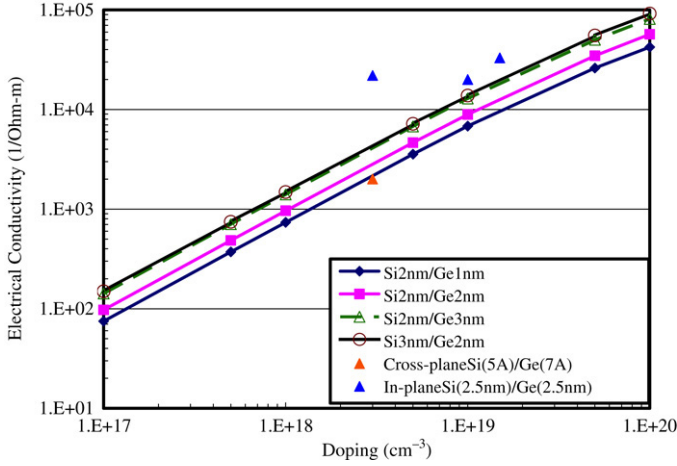
Fig. 10. Predicted and measured [93,96] electrical conductivity values for Si/Ge/Si superlattices.
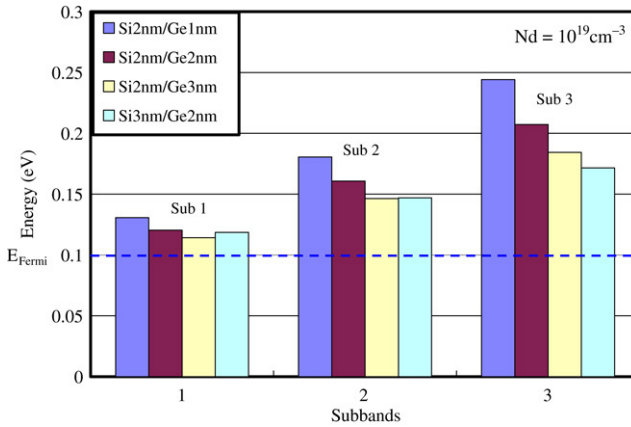


Fig. 11. Comparison of the first three subband energies of the Si/Ge/Si superlattices with varying thickness.

Fig. 10 shows the electrical conductivity values as a function of doping for the various superlattices and compared to measured values taken from [93,96]. In Fig. 10, for the silicon 2 nm superlattices, the electrical conductivity increases as a function of the germanium layer thickness. In addition, the conductivity of the Si(2 nm)/Ge(3 nm) superlattice is almost the same as the Si(3 nm)/Ge(2 nm) superlattice. The change in conductivity with superlattice thickness can be explained by looking at the subband energy levels in the various Si/Ge/Si superlattices as shown in Fig. 11. We compare the first three subband energies of the superlattices because the major contribution to transport in our simulations came from the conduction band and first three subbands.

In general, confinement of electrons increases the spacing between adjacent subband energy levels. For a constant silicon layer thickness of 2 nm, the subband energy of the germanium layers increases with decrease in germanium film thickness. The higher subband energy of the germanium 1nm layer results in an overall increase in the Si(2 nm)/Ge(1 nm) superlattice subband energies as is evident from Fig. 11 resulting in low electrical conductivity of this
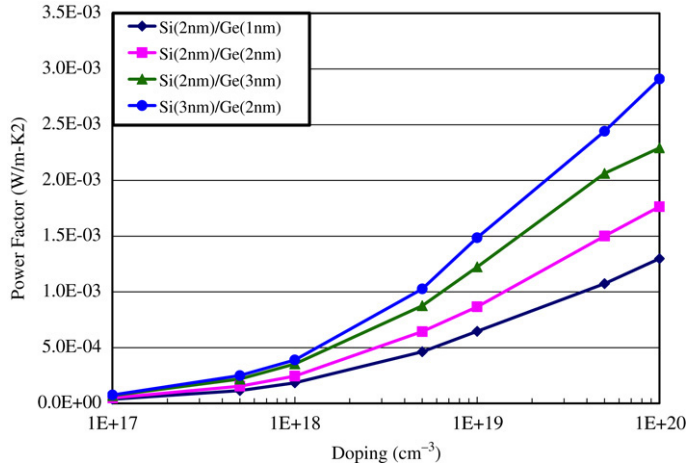
Fig. 12. Power factor of a 6 nm film predicted using the NEGF formalism.

superlattice. It can also be seen from Fig. 11 that the first two subband energies of the Si(2 nm)/Ge(3 nm) and Si(3 nm)/Ge(2 nm) superlattices are almost the same. The similar subband energies of these two superlattices causes their similar electrical performance as seen in Fig. 10.

The power factor of the superlattices is plotted in Fig. 12 as a function of doping for the various superlattices considered. As expected, the Si(3 nm)/Ge(2 nm) superlattice has the highest power factor due to its high electrical conductivity as well as a slightly higher Seebeck coefficient compared to the other superlattices. Of the Si(2 nm) layered superlattices with similar Seebeck coefficients, the superlattice with the germanium 1nm has the lowest power factor which is 47% lower than the superlattice with the germanium 3nm layer due to its low electrical conductivity. These results demonstrate the detrimental effects of quantum confinement at very small length scales.

## 6. Conclusion

Models based on Boltzmann and Fermi–Dirac statistics coupled in semi-classical transport have been very effective in identifying the pertinent physical parameters responsible for thermoelectric performance in bulk materials. In addition, the inclusion of various scattering mechanisms through the relaxation time approximation allow researchers to isolate and understand carrier scattering mechanisms that dominate thermoelectric performance for a particular temperature range. While the semi-classical models work well in predicting the performance of materials in the bulk regime, wave effects that cannot be captured inherently in particle-based models begin to dominate in nanostructured materials. Reduced dimensionality results in phonon confinement and formation of phonon bandgaps as well as tunneling and diffraction of electrons, characteristic of wave behavior. Furthermore, alteration of the dispersion relations of electrons and phonons at nanoscales affects the way these carriers interact with each other.

A quantum transport model that can successfully couple wave effects and scattering effects to predict thermoelectric performance is introduced through the non-equilibrium Green's function method. In addition to successfully coupling quantum and scattering effects, the NEGF method

allows us to seamlessly include various parameters that affect thermoelectric performance such as bandgaps, doping, and effective mass. The coupled thermoelectric solution combined with quantum effects demonstrates the capability of the NEGF method as a platform to design structures with enhanced figure of merit.

Reliance on Boltzmann-based models has produced a culture of "smaller is better" research, where the reduction in size is expected to produce limitless increases in performance. Experiments have not exhibited this behavior, and with a combined wave/particle model the apparent discrepancy can be explained. For materials at reduced scales, the governing physics changes enough that new models are required. The NEGF model suggests that optimization of devices is possible. Although this places theoretical upper limits on performance, there is no indication that these theoretical limits have been reached and continued research is warranted.

# References

 [1] T.J. Seebeck, Proc. Prussian Acad. Sci. (1822) 265–373.
 [2] J.C. Peltier, Ann. Chem. LVI (1834) 371–387.
 [3] W. Thomson, Proc. Roy. Soc. Edinburgh (1851) 91–98.
 [4] E. Altenkirch, Phys. Zeitschrift 10 (1909) 560–580.
 [5] E. Altenkirch, Phys. Zeitschrift 12 (1911) 920–924.
 [6] A.F. Ioffe, Semiconductor Thermoelements and Thermoelectric Cooling, Infosearch, London, 1957.
 [7] A.F. Joffe, Dokl. Akad. Naitk. USSR. 87 (1952) 369.
 [8] H.J. Goldsmid, Proc. Phys. Soc. London 67 (4) (1954) 360–363.
 [9] J. Bardeen, W. Shockley, Phys. Rev. 80 (1) (1950) 72–80.
[10] H.J. Goldsmid, R.W. Douglas, British J. Appl. Phys. 5 (11) (1954) 386–390.
[11] A.F. Ioffe, S.V. Airapetyants, A.V. Ioffe, N.V. Kolomoets, L.S. Stil'bans, Dokl. Akad. Nauk. USSR. 106 (1956) 981.
[12] U. Birkholz, Z. Naturforsch. 13a (1958) 780.
[13] F.D. Rosi, B. Abeles, R.V. Jensen, J. Phys. (c) 10 (1959) 191.
[14] W.M. Yim, F.D. Rossi, Solid State Electron. 15 (1972) 1121–1140.
[15] H.J. Goldsmid, in: T.M. Tritt (Ed.), Semiconductors and Semimetals, vol. 69, Academic Press, New York, 2001, p. 1.
[16] E.A. Skrabek, D.S. Trimmer, in: D.M. Rowe (Ed.), CRC Handbook of Thermoelectrics, CRC Press, Boca Raton, 1994.
[17] B. Abeles, D.S. Beers, G.D. Cody, J.P. Dismukes, Phys. Rev. 125 (1) (1962) 44–46.
[18] D.M. Rowe, C.M. Bhandari, in: Rhinehart Holt, Winston (Eds.), Modern Thermoelectrics, London, 1983.
[19] G.A. Slack, in: H. Ehrenreich, F. Seitz, D. Turnbull (Eds.), Solid State Physics, Academic Press, New York, 1979.
[20] D.G. Cahill, H.E. Fischer, S.K. Watson, R.O. Pohl, G.A. Slack, Phys. Rev. B. 40 (5) (1989) 3254–3260.
[21] S. Yamanaka, K. Kurosaki, A. Kosuga, K. Goto, H. Muta, Proc. Mat. Res. Soc. (Fall) (2005).
[22] G.S. Nolas, J.L. Cohn, G.A. Slack, Phys. Rev. B 58 (1998) 164.
[23] K. Hoang, S.D. Mahanti, J. Androulakis, M.G. Kanatzidis, Proc. Mat. Res. Soc. (Fall) (2005).
[24] R.F. Service, Science (2006) 1860.
[25] H. Bottner, G. Chen, R. Venkatasubramanian, Mat. Res. Soc. Bulletin 31 (2006) 211–217.
[26] A. Sommerfeld, Zeits. F. Physik 47 (1) (1928).
[27] A. Sommerfeld, N.H. Frank, Rev. Modern Phys. 3 (1) (1931) 1–8.
[28] F. Bloch, Zeits. F. Physik 52 (1928) 555.
[29] A.H. Wilson, Proc. Roy. Soc. London (A) 133 (822) (1931) 458–491.
[30] Bronstein, Phys. Z. Sowjetunion 2 (1932) 28.
[31] R.H. Fowler, Proc. Roy. Soc. London (A) 140 (842) (1933) 505–522.
[32] A.H. Wilson, Theory of Metals, Cambridge University Press, 1953.
[33] V.A. Johnson, K. Lark-Horovitz, Phys. Rev. 92 (2) (1953) 226–232.
[34] K. Lark-Horovitz, Middleton, Miller, Scanlon, Walerstein, Phys. Rev. 69 (1946) 259.
[35] Kelvin Lord, (Sir. W. Thomson) Collected Papers I, Cambridge University Press, 1882.
[36] L. Onsager, Phys. Rev. 37 (1931) 405.
[37] H.B. Callen, Phys. Rev. 73 (11) (1948) 1349–1358.

[38] H.P.R. Frederikse, Phys. Rev. 92 (2) (1953) 248–252.
[39] P.J. Price, Phys. Rev. 104 (5) (1956) 1223–1239.
[40] J. Tauc, Phys. Rev. 95 (6) ()(1954) 1394.
[41] L.E. Gurevich, J. Phys. (USSR) 9 (4) (1946) 26.
[42] R.P. Chasmar, R. Stratton, J. Electron. Control 7 (1959) 52–72.
[43] H. Littman, B. Davidson, J. Appl. Phys. 32 (2) (1961) 217–219.
[44] E.S. Rittner, G.F. Neumark, J. Appl. Phys. 34 (7) (1963) 2071–2077.
[45] R. Simon, J. Appl. Phys. 33 (5) (1962) 1830–1841.
[46] H.B. Callen, Phys. Rev. 76 (1949) 1394.
[47] H. Frohlich, Adv. Phys. 3 (1954) 325.
[48] Kohler, Z. Physik 125 (1948) 679.
[49] D.L. Rode, Phys. Rev. B 2 (4) (1970) 1012–1024.
[50] B.R. Nag, Electron Transport in Compound Semiconductors, Springer-Verlag, Berlin, 1980.
[51] E.O. Kane, J. Phys. Chem. Solids 1 (1957) 249.
[52] D.L. Rode, Phys. Rev. B 3 (10) (1971) 3287–3299.
[53] J.O. Sofo, G.D. Mahan, Phys. Rev. B 49 (7) (1994) 4565–4570.
[54] L. Esaki, R. Tsu, IBM J Res. Dev. (1970) 61–65.
[55] J.C. Slater, Phys. Rev. 87 (5) (1952) 807–835.
[56] L. Friedman, J. Phys. C Solid State Phys. 17 (1984) 3999–4008.
[57] A. Sibille, J.F. Palmier, H. Wang, F. Mollot, Phys. Rev. Lett. 64 (1) (1990) 52–55.
[58] H.T. Grahn, K. von Klitzing, K. Ploog, Phys. Rev. B 43 (14) (1991) 12094–12097.
[59] S.K. Lyo, Phys. Rev. B 38 (9) (1988) 6345–6347.
[60] S.S. Kubakaddi, B.G. Milimani, P.N. Butcher, Sem. Sci. Tech. 7 (1992) 1344–1349.
[61] S.Y. Mensah, G.K. Kangah, J. Phys. Condens. Matter 4 (1992) 919–922.
[62] L.D. Hicks, M.S. Dresselhaus, Phys. Rev. B 47 (19) (1993) 12727–12731.
[63] J.O. Sofo, G.D. Mahan, Appl. Phys. Lett. 65 (21) (1994) 2690–2692.
[64] D.A. Broido, T.L. Reinecke, Phys. Rev. B 51 (19) (1995) 13797–13800.
[65] D.A. Broido, T.L. Reinecke, Phys. Rev. B 64 (2001) 045324.
[66] B.R. Nag, Electron Transport in Compound Semiconductors, Springer-Verlag, Berlin, 1980.
[67] T.J. Scheidemantel, C. Ambrosch-Draxl, T. Thonhauser, J.V. Badding, J.O. Sofo, Transport coefficients from first-principles calculations, Phys. Rev. B 68 (2003) 125210.
[68] S. Lee, P. von Allmen, Appl. Phys. Lett. 88 (2006) 022107.
[69] A. Balandin, K.L. Wang, Phys. Rev. B 58 (3) (1998) 1544–1549.
[70] A. Balandin, K.L. Wang, J. Appl. Phys. 84 (11) (1998) 6149–6153.
[71] L.D. Hicks, T.C. Harman, M.S. Dresselhaus, Appl. Phys. Lett. 63 (22) (1993) 3230–3232.
[72] L.W. Whitlow, T. Hirano, J. Appl. Phys. 78 (9) (1995) 5460–5466.
[73] M.S. Dresselhaus, Nanostructures and energy conversion, in: Proc. of 2003 Rohsenhow Symposium on Future Trends of Heat Transfer, Cambridge, MA.
[74] T. Koga, S.B. Cronin, M.S. Dresselhaus, J.L. Liu, K.L. Wang, Appl. Phys. Lett. 77 (10) (2000) 1–3.
[75] M.S. Dresselhaus, Y.M. Lin, T. Koga, S.B. Cronin, O. Rabin, M.R. Black, G. Dresselhaus, in: T.M. Tritt (Ed.), Semiconductors and Semimetals, III, Academic Press, New York, 2001.
[76] S. Datta, Superlattices and Microstructures 28 (2000) 253–278.
[77] S. Datta, Quantum Transport: Atom to Transistor, Cambridge University Press, New York, 2005.
[78] A. Bulusu, D.G. Walker, J. Heat Transfer 129 (2007).
[79] A. Bulusu, D.G. Walker, IEEE Trans. Electron. Dev. 55 (2008) 423–429.
[80] A. Bulusu, D.G. Walker, J. Appl. Phys. 102 (7) (2007).
[81] A. Szafer, A.D. Stone, Phys. Rev. Lett. 62 (1989) 300–303.
[82] M. Lundstrom, Fundamentals of Carrier Transport, Cambridge University Press, 2000.
[83] L.D. Hicks, M.S. Dresselhaus, Phys. Rev. B 47 (19) (1993) 12727–12731.
[84] J.H. Choi, Y.J. Park, H.S. Min, IEEE Elect. Dev. Lett. 16 (11) (1995) 527–529.
[85] S. Takagi, J. Koga, A. Toriumi, IEEE Trans. Intl. Elect. Dev. Meet. (1997) 219–222.
[86] T. Wang, T.H. Hsieh, T.W. Chen, J. Appl. Phys. 74 (1) (1993) 426–430.
[87] V.A. Fonoberov, A.A. Balandin, Nano Lett. 6 (11) (2006) 2442–2446.
[88] D. Vashaee, A. Shakouri, J. Appl. Phys. 95 (3) (2004) 1233–1245.
[89] A. Asenov, J.R. Watling, A.R. Brown, D.K. Ferry, J. Comput. Elect. 1 (2002) 503–513.
[90] T.W. Tang, B. Wu, Semi. Sci. Tech. 19 (2004) 54–60.
[91] B. Yang, W.L. Liu, J.L. Liu, K.L. Wang, G. Chen, Appl. Phys. Lett. 81 (19) (2002) 3588–3590.

[92]  R. Muller, T. Kamins, M. Chan, Device Electronics for Integrated Circuits, Wiley, New York, 1986.

[93]  B. Yang, J.L. Liu, K. Wang, G. Chen, Proc. Mat. Res. Soc. 691 (2002) G.3. 2.1–2.6.

[94]  B. Yang, J.L. Liu, K.L. Wang, G. Chen, Appl. Phys. Lett. 80 (10) (2002) 1758–1760.

[95]  W.L. Liu, T.B. Tasciuc, J.L. Liu, K. Taka, K.L. Wang, M.S. Dresselhaus, G. Chen, Intl. Conf. on Thermoelectrics, 2001, pp. 340–343.

[96]  R. Venkatasubramanian, T. Colpitts, E. Watko, D. Malta, Proc. Spring Meet. Mat. Res. Soc. (1997).